Across-arc variations in K-isotope ratios in lavas of the Izu arc: Evidence for progressive depletion of the slab in K and similarly mobile elements

Christopher A. Parendo* [1], Stein B. Jacobsen [1], Jun-Ichi Kimura [2], Rex N. Taylor [3]

Affiliations:

[1] Department of Earth and Planetary Sciences, Harvard University, US

[2] JAMSTEC, Yokosuka, Japan

[3] School of Ocean and Earth Science, University of Southampton, UK

*Correspondence to: cparendo@fas.harvard.edu

Abstract:

In subduction zones, fluids rise from the slab to the mantle, causing metasomatism and flux melting of the mantle to produce arc magmas. The transfer of material from slab to mantle and, in turn, to arc crust is an important control on the long-term chemical evolution of the mantle and continental crust. In this study, we investigate the transport of K in subduction zones, by exploring the systematics of K stable-isotope variations in lavas of the Izu arc. We find that the Izu lavas have isotopically heavy K, relative to estimates for midocean ridge basalt (MORB)-source upper mantle. Moreover, the $\delta^{41}\mathrm{K}$ values of the lavas are clearly heavier than those of subducting sediments and are probably heavier than subducting altered ocean crust. An across-arc decrease in $\delta^{41}\mathrm{K}$ values is apparent. Arc-front lavas are heavier than the mantle by about 0.22‰ (median), whereas rear-arc lavas are heavier by only about 0.08‰ (median). The heavy K-isotope compositions of the arc lavas may arise from isotopic fractionation during slab dehydration, where light K is preferentially retained in phases such as phengite in the slab. The across-arc decrease in $\delta^{41}\mathrm{K}$ values is due to progressive breakdown of these phases, and to associated depletion of the slab in heavy K. Variations in the relative contributions of different source materials—igneous ocean crust, sediment, and mantle peridotite—may also play a role. In particular, we explore one possibility, motivated by radiogenic-isotope studies, that the slab signal in K isotopes may be attenuated in the rear arc as a result of extensive fluid-mantle interaction. If K isotopes do track slab dehydration, then K isotopes provide insight into the transfer of K and similarly mobile elements out of the slab and into the upper mantle and arc

crust. Lastly, we observe extreme isotopic variations in some of the lavas, which we interpret to result from crustal-level processes that affect only a subset of the lavas.

1. Introduction

The chemical compositions of arc lavas provide insights into the unique processes occurring in subduction zones. Arc lavas are typically enriched in large-ion lithophile elements (LILEs; K, Rb, Sr, Cs, Ba, and light REEs) and other fluid-mobile elements (e.g., Pb). These enrichments are presumed to reflect fluid-transport processes. Specifically, transfer of fluids—whether aqueous solutions or hydrous melts (Keppler, 2017; Spandler and Pirard, 2013)—from the subducting slab to the overlying mantle is expected to enrich the mantle wedge in these elements. Partial melting of the metasomatized mantle wedge produces magmas, enriched in these elements, that ultimately erupt from arc volcanos.

Potassium is among the elements that exhibit a marked enrichment in arc lavas—and is likely centrally involved in processes of dehydration, melting, and fluid transport in the slab and mantle. At pressure and temperature conditions of the slab at subarc depths, K is hosted in the mica mineral phengite (Hermann and Rubatto, 2009; Hermann and Spandler, 2008; Schmidt et al., 2004). Since phengite is also an important host of H_2O and many LILEs, the behavior of K in subduction zones is coupled, to some degree, to that of H_2O and select LILEs—particularly, Ba, Cs, and Rb. As slab-derived aqueous solutions or hydrous melts rise into the mantle, there is also potential for interaction between these fluids and mantle peridotite. This may entail precipitation or dissolution of the K-bearing mica mineral phlogopite (Pirard and Hermann, 2015;

Sekine and Wyllie, 1982), which, like phengite, hosts H_2O and LILEs. Better understanding of the behavior of K is therefore likely to provide general insights into the material transport of H_2O, LILEs, and fluid-mobile elements in subduction zones.

Stable K-isotope ratios of arc lavas have the potential to place new constraints on the transport of K in subduction zones. Heterogeneities in K-isotope compositions have been documented within, and among, pertinent reservoirs including the upper mantle (Tuller-Ross et al., 2019a), altered oceanic crust (Parendo et al., 2017; Santiago Ramos et al., 2020) and marine sediments (Hu et al., 2020; Parendo et al., to be submitted). Additionally, isotopically light K has been observed in samples of exhumed eclogite—and, specifically, in mineral separates of phengite—suggesting that slab dehydration results in fractionation of K isotopes (Liu et al., 2020). Recently, Hu et al. (2021) reported covariation between K-isotope ratios and radiogenic isotopes in lavas from the Lesser Antilles arc, consistent with variable addition of K to the mantle from isotopically light subducted sediments. Thus, K-isotope variations in arc lavas may reflect isotopically distinct source materials or isotopic fractionation in association with fluid-transport processes.

Here we report K-isotope data for volcanic samples from the Izu arc. Potassium-isotope data are here expressed as parts per thousand deviations relative to the standard NIST SRM 3141a. That is, $\delta^{41/39}K = [(^{41}K/^{39}K)_{sample}/(^{41}K/^{39}K)_{SRM3141A} - 1]*10^3$. The sample set includes materials from both the arc front and rear arc, such that across-arc variations can be evaluated (**Figure 1**). We explore possible explanations for observed across-arc variations in K-isotope ratios. In particular, we consider the influence of (1) different source materials (i.e., mantle

65 wedge, sediment, and altered ocean crust), and (2) progressive breakdown of phengite and
66 depletion of the slab in K

67

68 **2. Analytical methods**

69

70 *Sample Processing*

71

72 Most samples were received as powders. Data previously obtained for these samples were
73 presented in Taylor and Nesbitt (1998) and Kimura et al. (2010). A small number of samples—
74 including all samples of highly altered subaqueous lavas—were received as rock fragments.
75 These were powdered in an agate mortar or alumina shatterbox.

76 Dissolutions were performed using HF, HNO_3 and HCl saturated hydrofluoric, nitric and
77 hydrochloric acids, respectively. Aliquots of sample powders (40-80 mg) were weighed out and
78 transferred to 30 mL Savillex PFA beakers. A mixture of 0.5 mL HF, 2 mL HNO_3, and 1 mL HCl
79 acids was added to each, and the capped beakers were heated at 170°C on a hotplate for one or
80 more days. The resulting solutions were dried down, then redissolved in a mixture of 0.5 mL
81 HNO_3, 1.5 mL HCl, and 1 mL H_2O. Again, these were heated for at least one day. After complete
82 dissolution, the samples were stored in 4 mL 3N HNO_3.

83 Potassium was isolated by ion-exchange chromatography. Quartz-glass columns, with 0.4
84 cm inner diameter, were filled with 1.63 mL Bio-Rad AG50-X8 (100-200 mesh) ion-exchange resin.
85 The resin was cleaned with 100 mL 4N HCl, rinsed with 10 mL purified H_2O, and conditioned with
86 20 mL 0.5N HNO_3. Dissolved samples containing 10-100 ug K were loaded onto the resin in 0.5

mL 0.5N HNO_3. Next, a volume of 49 mL 0.5N HNO_3 was passed through each column, and K was collected in the interval from 24-49 mL. This step was repeated, such that all samples were passed through the columns twice. The purified K was then dissolved in 2% HNO_3, by volume, in preparation for analysis by MC-ICPMS.

Potassium Isotopic Analysis

Potassium isotope analyses were generated using a Nu Sapphire MC-ICPMS equipped with a hexapole collision-and-reaction cell. Additional details on data acquisition are provided in **Supplement**. Isotope ratios were determined by the standard-sample bracketing method. A lab standard (abbreviated to "Suprapur") derived from a batch of Merck KgaA Suprapur KNO_3 was used as the bracketing standard. Data are reported in delta notation relative to the NIST SRM 3141a. Values were converted to the NIST SRM 3141a scale by use of the following conversion: $\delta^{41}\mathrm{K}_{\text{Relative to SRM 3141a}} = \delta^{41}\mathrm{K}_{\text{Suprapur}} - 0.047$ (Supplement).

Analytical uncertainty is estimated from replicate analyses of standards. In this report, we use "N" to denote the number of analytical sessions; and "n" the number of bracketed analyses of a sample solution during a particular session. The long-term reproducibility of NIST SRM 3141a solutions, which were not processed through columns, was 0.02‰ (2SD, N=45). External reproducibility was estimated by processing rock standards through chromatographic columns and analyzing the purified K solutions multiple times: Geological Survey of Japan standards JA-1 and JA-2 were reproducible at levels of 0.03‰ (2SD, N=4) and 0.04‰ (2SD, N=18),

respectively. We consider the latter value (0.04‰, 2SD) to be a reasonable estimate of the uncertainty associated with the $\delta^{41}K$ values reported for our samples.

3. Results

Potassium-isotope data for the arc-front and rear-arc lavas, and for variably altered arc materials, are provided in the Supplement and summarized in **Figure 2**. We make three main observations.

First, we observe that materials from the Izu arc have $\delta^{41}K$ values that are generally heavy, relative to estimates of the upper mantle, and relative to many subduction inputs (**Figure 3)**. The $\delta^{41}K$ values of the arc-front lavas have a median of -0.22‰ and largely cluster between -0.26‰ and -0.18‰ (25th and 75th percentiles). The $\delta^{41}K$ values of the rear-arc lavas have a median of -0.36‰ and mostly cluster between -0.40‰ and -0.29‰ (25th and 75th percentiles). These values for the arc front are higher than estimates for the upper mantle based on analyses of MORBs and other mantle-derived products: Tuller-Ross et al. (2019a) reported a mean $\delta^{41}K$ value of -0.44‰ ± 0.09‰ (1SD) for a set of 32 MORB samples. The values for the rear arc are also slightly heavier than the MORB average, though the difference is small and not necessarily significant.

Second, we observe an across-arc decrease in $\delta^{41}K$ values, with heavier values in the arc front and lighter values in the rear arc. To make this apparent, we plot the distributions of $\delta^{41}K$ values from the arc front and rear arc (**Figure 3**). Despite high variability among some materials, the distributions appear to be offset from one another. To formalize this observation, we note that the median $\delta^{41}K$ of the arc front lavas is greater than that of the rear-arc lavas by 0.14‰,

and that a bootstrapping calculation yields an estimated 95% confidence interval for this difference of 0.08 to 0.20‰ (**Supplement**). In describing these data, we have used medians rather than means since the median statistic is not as sensitive to outlier values.

Third, we observe that a subset of the samples from the arc front and rear arc are extremely variable. In the arc front, most samples have similar $\delta^{41}K$ values, but one sample has a $\delta^{41}K$ value of -0.65‰, which is far lower than the rest. In the rear arc, again most samples have $\delta^{41}K$ values that fall within a narrow range; however, several samples (7 or 8) are highly variable, with $\delta^{41}K$ values as low as -0.81‰ and as high as +0.88‰.

Lastly, we note that the $\delta^{41}K$ values of visibly altered materials from the submerged caldera Omuradashi are somewhat more variable, and extend to slightly heavier values, in comparison to the $\delta^{41}K$ values of the samples from subaerial lavas of the arc front (**Figure 2**).

4. Discussion

4.1.1. Possible sources of isotopically heavy K

A central finding of this study is that the lavas of the arc front are isotopically heavy. A source of heavy K to the arc front is therefore required. In the following, we consider two possibilities. First, we consider whether any of the reservoirs within the subduction zone has sufficiently heavy K to account for the arc-front compositions. We conclude that this is possible only if the K-isotope composition of lower oceanic crust, which is not well characterized, is heavy. Second, we consider whether isotopic fractionation occurs in association with slab dehydration and/or

152 melting. In the context of the Izu arc, isotopic fractionation as a result of dehydration processes
153 has been proposed for other stable-isotope systems—in particular, for U, W, and Mo stable-
154 isotope ratios (Freymuth et al., 2019; Mazza et al., 2020; Villalobos-Orchard et al., 2020). In our
155 view, it is also possible that K-isotope ratios are significantly fractionated in sub-arc settings.
156
157 4.1.2. Isotopic composition of slab and mantle wedge
158
159 Potassium from neither the mantle wedge nor from sediments is likely to be sufficiently heavy to
160 account for the K-isotope values of the arc-front lavas. We assume that the mantle wedge has a
161 K-isotope composition that is similar to the MORB-source upper mantle. Available data for
162 MORBs indicate an average $\delta^{41}\mathrm{K}$ value of -0.44 ± 0.09‰ (1SD; n = 32; Tuller-Ross et al., 2019).
163 This value should reflect the composition of the MORB source. An isotopic offset between MORB
164 and the MORB-source upper mantle is unlikely because K partitions nearly quantitatively into the
165 liquid during partial melting to produce MORB. Thus, we assume that the mantle wedge has a
166 composition similar to that of MORBs. The K-isotope composition of sediments is constrained by
167 analyses of sediments from IODP Site 1149 adjacent to the Izu trench. Data for these sediments
168 indicate an average $\delta^{41}\mathrm{K}$ value of -0.53 ± 0.06‰ (1SD; n = 19; Parendo et al., under review;
169 Supplement). In addition, variability in $\delta^{41}\mathrm{K}$ values with depth in the sediment column is limited:
170 The average values by lithological unit are -0.53‰ in Unit I (n = 8), -0.54‰ in Unit II (n = 3), -
171 0.58‰ in Unit III (n = 3), and -0.51‰ in Unit IV (n = 5). Thus, the K of both the mantle wedge and
172 subducting sediments is estimated to be too light to explain the heavy K of the arc-front lavas.

The upper part of oceanic crust—which acquires K from interaction with seawater—also does not appear to be very isotopically heavy. Two K-isotope studies have included samples of altered oceanic crust from Site 801 in the western Pacific. Materials recovered from this site include altered basalts from the upper approximately 400 m of a MORB section. In one study, an average $\delta^{41}\mathrm{K}$ value, weighted by K/Ti ratios, was reported of -0.36 ± 0.18‰ (1SD; n = 12; Santiago Ramos et al., 2020). In another study, a 'super composite' from Site 801 (Kelley et al., 2003) was among the materials analyzed: the composite was reported to have $\delta^{41}\mathrm{K}$ value of -0.32 ± 0.04‰ (2SD; analytical uncertainty; Hu et al., 2020). Both estimates suggest that the upper part of oceanic crust at this site has a $\delta^{41}\mathrm{K}$ value that is similar to or about 0.1‰ heavier than the MORB average. Similar observations have come from analyses of materials from the upper part of the Troodos ophiolite (Santiago Ramos et al., 2020) and Sites U1365 and U1368 in the South Pacific (Liu et al., 2021). Altered oceanic crust—at least the upper few hundred meters—may be slightly heavier than MORB but is probably not sufficiently heavy to explain the arc-front lavas.

Few data are available to characterize lower oceanic crust. Parendo et al. (2017) reported analyses of a set of samples (n = 6) from the Bay of Islands ophiolite. The materials derive from relatively deep parts of the oceanic crustal section. The 4 samples of altered basalts and diabases (i.e., excluding analyses of an unaltered gabbro and a plagiogranite) have a range in $\delta^{41}\mathrm{K}$ values from 0.22 to -0.06‰ (**Figure 3**). If these values are representative of lower oceanic crust, then this could serve as a source of heavy K. However, there are significant uncertainties. For example, the materials of the Bay of Islands ophiolite have highly elevated $^{87}Sr/^{86}Sr$ ratios. This may be common among ophiolites (Alt and Teagle, 2000; Coogan, 2009). But the $^{87}Sr/^{86}Sr$ ratios are more elevated than what appears to be typical of lower-crustal materials obtained by drilling

195 in modern oceanic crust at locations such as Site 504 in the eastern Pacific (Alt and Teagle, 2000).
196 Thus, the Bay of Islands materials may reflect greater interaction between seawater and oceanic
197 crust than is typical. Lower oceanic crust offers a potential—but presently uncertain—source of
198 heavy K.

199 We note that, although sediments and upper altered ocean crust are high in K relative to
200 MORB (or to lower-oceanic crust), it is nonetheless plausible that a significant fraction of K in the
201 Izu lavas derives from lower crust. Increasingly, models of slab dehydration invoke fluid loss from
202 hydrated peridotite, including from peridotite that is part of the mantle wedge near the slab-
203 wedge interface, and from peridotite that comprises the base of the subducting slab (e.g.,
204 Spandler and Pirard, 2013). If aqueous solutions are released by dehydration of peridotite in the
205 slab, these fluids will rise through the entire thickness of the oceanic crust, potentially
206 incorporating material from lower oceanic crust, upper oceanic crust, or sediments. Pertinently,
207 $^{206}Pb/^{204}Pb$ and $^{208}Pb/^{204}Pb$ ratios in the Izu arc lavas may require a large contribution of Pb
208 specifically from lower oceanic crust, as upper oceanic crust has high $^{206}Pb/^{204}Pb$ ratios (reflecting
209 U addition by seawater and radiogenic ingrowth) that make it unsuitable as a significant
210 component to the Izu lavas (Freymuth et al., 2019). Thus, future work investigating the K-isotope
211 composition of lower oceanic crust will be valuable in assessing this reservoir as a source of heavy
212 K to the Izu arc. In the following section, we consider an alternative explanation for the origin of
213 heavy K in the Izu lavas.
214
215 4.1.3. Isotopic fractionation in association with slab dehydration or melting
216

Potassium is likely to be retained in the slab as phengite—or possibly in the mantle wedge as phlogopite—and this may provide a mechanism to fractionate K isotopes. The expression of isotopic fractionation in a slab-derived fluid phase requires that a significant fraction of an element be retained in a solid phase. As examples, the U-isotope compositions of the Izu arc-front lavas have been proposed to arise via retention of U in slab-hosted epidote, apatite, or zircon (Freymuth et al., 2019). Likewise, W- and Mo-isotope compositions of the arc-front lavas have been provisionally associated with retention of these elements in rutile (Mazza et al., 2020; Villalobos-Orchard et al., 2020). In the case of K, experiments indicate that the primary host in the slab at sub-arc conditions is likely phengite (Schmidt et al., 2004; Hermann and Rubatto, 2009). In addition, phlogopite may be stabilized in the mantle if K-rich fluids interact extensively mantle-wedge peridotite (Sekine and Wyllie, 1982). If K isotopes are fractionated in subduction zones, it likely occurs because of retention of K in slab-hosted phengite or in mantle-hosted phlogopite.

An open question is whether fractionation effects on $^{41}K/^{39}K$ ratios will be of significant magnitude at the high-temperature conditions of the sub-arc slab or slab-mantle interface. Equilibrium isotope effects are likely to be small at these conditions. Ab initio calculations provide estimates for equilibrium fractionation factors for several K-bearing minerals and aqueous K (Li et al., 2019; Zeng et al., 2019). No such estimates are available specifically for phengite or fluids at high pressure-temperature conditions. Nonetheless, the magnitude of effects as estimated by Zeng et al. (2019) among silicate phases—including orthoclase, illite, muscovite, and phlogopite—and dilute aqueous K are small at high temperatures. The effects among these specific phases would be on the order of 0.05‰ or less at temperatures of 700-

800°C—i.e., at temperatures corresponding to an estimate of the slab surface temperature under the Izu arc (Syracuse et al., 2010). These estimates suggest that equilibrium-isotope fractionation will not produce sufficiently fractionated K-isotope ratios to explain the heavy K in the Izu arc front.

More significant isotope effects may arise through kinetic processes, though the particular mechanism here is uncertain. Isotopically light K has been noted in one study of eclogitic materials, including K-bearing amphibole and phengite (Liu et al., 2020). The eclogites of that study—from the Sumdo metamorphic belt in Tibet—have a mean K-isotope composition that is about -0.76‰, which is about 0.32‰ lower than average MORB. This offers general support for the possibility of significant isotopic fractionation occurring in the slab. In our view, one potential opportunity for kinetic effects to arise is through (re-)precipitation of K as phengite in veins or as phlogopite near the slab-mantle interface. Phengite can be an important component of ecologitic veins (Spandler and Hermann, 2006), and phlogopite may precipitate where slab-derived fluids infiltrate the mantle (Sekine and Wyllie, 1982). Unidirectional transfer of an element from one phase (e.g., a fluid) to another (e.g., phengite or phlogopite) may result in kinetic isotope fractionation with preferential transfer of lighter isotopes—especially if diffusion in some way limits the rate of transfer of an element. Whether a process like this affects K isotopes in subduction zones is speculative, but we note it as one potential mechanism that could result in lighter K in phengite or phlogopite and heavier K in a corresponding fluid.

4.2.1. Possible causes of across-arc K-isotope variation

Another important finding of this study is the across-arc decrease in $\delta^{41}K$ values—at least when comparing median compositions. While the arc front is distinctly heavy, the rear arc is similar to or only slightly heavier than MORB. A number of other geochemical parameters also exhibit a systematic across-arc difference. These include trace-element ratios that are often interpreted as indicating a fluid component (Ba/Th) versus a melt or sediment component (La/Sm). These also include stable- and radiogenic-isotope ratios. In the following, we discuss specific mechanisms that may account for the across-arc shift in $\delta^{41}K$ values within the context of these constraints.

4.2.2. Across-arc breakdown of K-bearing phases

Progressive breakdown of K-bearing phases such as phengite in the slab may account for the across-arc decrease in K-isotope ratios. In previous sections, we noted that in our view the heavy K of the arc-front lavas implies that isotopic fractionation may occur such that K in the fluid phase is heavy relative to K in the mineral phases. If this is correct, then it follows that the K-isotope compositions of slab-derived fluids will decrease as increasing amounts of phengite (or other K-bearing phases) are dissolved into aqueous solutions or hydrous melts. This dynamic may arise in two ways. First, it may occur because of a simple distillation effect. Namely, if heavy K is lost under the arc front, the residual slab will be isotopically light. Fluids derived from it will presumably reflect this lighter composition. Second, it may occur in response to an increase in the solubility of phengite. The solubility of phengite increases with temperature, especially as the solidus is crossed (Hermann and Spandler, 2006; Hermann and Spandler, 2009). If phengite

283 dissolves extensively, then a greater proportion of K will be transferred to the fluid. In this case,
284 the K-isotope composition of the fluid will more closely resemble the composition its source. To
285 summarize, if K isotopes are fractionated during slab dehydration or melting, then the
286 progressive breakdown of phengite or other K-bearing phases may result in increasingly light K
287 being released from the slab as it descends.

288 An isotopic signal from progressive depletion of the slab in heavy K—and/or greater
289 partitioning of K into a fluid under the rear arc—is qualitatively consistent with many other
290 geochemical parameters. In particular, the Izu arc front is characterized by high Ba/Th, Pb/Ce,
291 and Cs/Rb ratios. The high relative abundances of fluid-mobile elements (e.g., Ba, Pb, and Cs) in
292 the arc front has been attributed to a significant influence by slab-derived aqueous fluids rather
293 than (or in addition) to a slab-derived melts. The rear-arc exhibits lesser relative enrichments in
294 these elements, suggesting a stronger influence by slab-derived melts. These observations may
295 be reconciled with a model in which K is more completely dissolved in the rear arc, resulting in a
296 fluid with a K-isotope composition more directly reflective of its source. Alternatively, some of
297 the across-arc decrease in the relative abundances of Ba, Pb, and Cs may arise from the depletion
298 of the slab in these readily mobilized elements. In particular, across-arc variations in Cs/Rb and
299 Cs/K ratios in arc lavas have been hypothesized to result from depletion of the slab in Cs relative
300 to Rb and K, specifically as a consequence of the relative compatibilities of these elements in
301 phengite (Melzer and Wunder, 2000). Cesium is highly incompatible, whereas Rb and K are both
302 compatible in phengite (Melzer and Wunder, 2000; Hermann and Rubatto, 2009). Thus, the
303 across-arc decreases in the relative abundances of fluid-mobile elements appear also to be

304 consistent with progressive loss of material from the slab—and an associated fractionation of
305 trace-element and possibly K-isotope ratios.

306 Other stable-isotope systems also seem to exhibit across-arc changes. However, as a
307 general matter, the number of analyses of rear-arc samples is limited. Uranium is similar to K in
308 its level of enrichment in the Izu arc-front and rear-arc lavas relative to other trace elements.
309 Hence, U and K may be surmised to behave analogously—or at least to be similarly mobile in this
310 subduction zone. Freymuth et al. (2019) observed that U-isotope ratios ($^{238}U/^{235}U$) are very light
311 in the arc front and interpreted these values as reflecting isotopic fractionation as U partitions
312 into an aqueous fluid. By contrast, U-isotope ratios from the rear-arc island of Niijima (n = 2) are
313 more similar in composition to estimates for slab components such as sediment or MORB. This
314 is consistent with the fullest expression of isotopic fractionation occurring in the arc front where
315 an aqueous-fluid influence may be especially strong. In the model of Freymuth et al. (2019), it is
316 assumed that U isotopes are negligibly fractioned in slab melts—i.e., a fractionation factor (α) of
317 one. A difference in the fractionation factor that characterizes partitioning into aqueous fluids
318 versus into melts is one valid explanation for across-arc isotopic changes. Progressive depletion
319 of the slab—or more quantitative transfer of elements into the liquid phase—is another, as we
320 have emphasized for K isotopes.

321

322 4.2.2. Across-arc changes in source of K

323

324 Here, we consider across-arc changes in the source of materials to the Izu lavas. We focus on
325 constraints from radiogenic-isotope systems, though interpretations of these systems are varied.

We note, first, that $^{143}Nd/^{144}Nd$ and $^{176}Hf/^{177}Hf$ ratios are slightly less radiogenic in the rear arc, consistent with a more enriched reservoir. This may reflect an input by a sediment-melt component to the rear arc or compositional heterogeneity in the mantle wedge. On the other hand, $^{206}Pb/^{204}Pb$ and $^{87}Sr/^{86}Sr$ ratios are less radiogenic in the rear arc, consistent with a more depleted reservoir. This may reflect a greater contribution of these elements by mafic-oceanic crust or by the mantle wedge. In the following, we consider K-isotope variations primarily in relation to Pb- and Sr-isotope ratios. We illustrate these considerations with two models. In the first, slab-derived fluids dominate the signal in Pb-, Sr-, and K-isotope ratios in both the arc front and rear arc. In the second, the slab signal is attenuated in the rear arc as a result of a greater mantle-wedge contribution of Pb, Sr, and K.

To start, we note that K, Pb, and Sr are present at high concentrations in the Izu lavas, relative to MORB compositions, such that each of these elements appears to have been vastly enriched in the source region of the Izu arc by the action of metasomatic fluids. Enrichment of K in the Izu lavas can be illustrated by K/Yb – Nb/Yb systematics (Pearce, 1982). In a K/Yb – Nb/Yb diagram, MORB compositions define an array (**Figure 5a**), where most of the variance is interpreted to result from (1) mantle heterogeneity and (2) variable degrees of partial melting (Pearce, 1982). Assuming that the Yb and Nb contents of the mantle wedge are negligibly affected by fluids, displacements from the MORB array in K/Yb – Nb/Yb space are attributed entirely to additions of K to the mantle by metasomatic fluids. As illustrated, the K/Yb ratios of the Izu lavas are elevated relative to the MORB array, by factors of roughly 16 in the arc front, and 8 in the rear arc (**Figure 5a**). These enrichment factors translate into estimates that metasomatic fluids account for about 94% of the K in the arc front lavas, and about 88% of the K

348 in the rear arc lavas (**Figure 5b**). Analogous systematics show that Pb and Sr are also vastly
349 enriched in the Izu lavas (**Figure 5b**). By contrast, the much smaller enrichments in Nd and Hf
350 abundances imply that lower proportions of these elements are contributed by metasomatic
351 fluids; accordingly, Nd and Hf isotopic variations in the lavas may largely reflect mantle
352 heterogeneities (Straub et al., 2010). Thus, in assessing the effect of changes in source materials
353 on the K-isotope compositions of the Izu arc lavas, we focus on the Pb and Sr radiogenic-isotope
354 systems, since the Pb, Sr, and K contents of the lavas appear to be principally controlled by
355 metasomatic fluids.

356 The Pb- (and Sr-) isotope systematics of the Izu arc have been interpreted in two
357 fundamentally different ways. In one view, the unradiogenic—low $^{206}Pb/^{204}Pb$—endmember in
358 mixing relationships is the mantle wedge. The basis for identifying the mantle as the source of
359 unradiogenic Pb is that $^{208}Pb/^{204}Pb$ vs. $^{206}Pb/^{204}Pb$ require that the unradiogenic component have
360 high $^{208}Pb/^{204}Pb$ at a given $^{206}Pb/^{204}Pb$ ratio. That is, the unradiogenic component must have an
361 Indian-Ocean-Type Pb-isotope signature. The mantle wedge appears to have an Indian-Ocean-
362 Type signature (Hickey-Vargas, 1991; Hickey-Vargas, 1998). By contrast, mafic oceanic crust
363 adjacent to the Izu trench has a Pacific-Ocean-Type Pb-isotope signature (Hauff et al., 2003;
364 Durkin et al., 2020). On this basis, several studies have identified the mantle wedge as a
365 significant source of unradiogenic Pb. These studies have interpreted the relatively unradiogenic
366 Pb (and Sr) in the rear arc as indicative of a greater proportion of mantle-derived Pb (and Sr) in
367 those lavas (Hochstaedter et al., 2001; Ishizuka et al., 2006; Kimura et al., 2010; Taylor and
368 Nesbitt, 1998; Tollstrup et al., 2010).

Alternatively, it has been proposed that the mantle wedge is incapable of supplying a large proportion of Pb to the Izu arc lavas, so that subducting mafic oceanic crust must serve as the depleted endmember. Straub et al. (2009) pointed out that simple mixing of slab-derived fluids with mantle peridotite is insufficient as a mechanism to explain both the Pb enrichments and the Pb-isotope compositions of the lavas. To illustrate this: in a simple mixing scenario, Pb-isotope data would require that roughly 50% of Pb in the rear-arc lavas be derived from the mantle, whereas Pb/Yb – Nb/Yb systematics would require that roughly 90% of the Pb in the same lavas be supplied by an external source, presumably slab-derived fluids (**Figure 5b**). This is a severe inconsistency. Thus, Straub et al. (2009) proposed that mafic oceanic crust must be the dominant source of the unradiogenic Pb. Accordingly, it was inferred that the subducted oceanic crust has an Indian-Ocean-type Pb-isotope composition Straub et al. (2009; 2010). The strength of this interpretation is that it reconciles the Pb-isotope and the elemental relationships. Yet, this interpretation requires that oceanic crust presently under the Izu arc have a fundamentally different Pb-isotope signature as compared to the oceanic crust presently adjacent to the Izu trench. This is a possibility but has not been substantiated by independent evidence.

4.2.3. Model 1: Control of K, Pb, and Sr by slab components

Here, we consider a model in which the slab components explain the Pb, Sr, and K contents of the Izu lavas. We adopt the assumption that the mafic oceanic crust of the subducting slab has an Indian-Ocean-type radiogenic-isotope signature, as proposed by Straub et al. (2009; 2010). In this scenario, the less radiogenic $^{206}Pb/^{204}Pb$ and $^{87}Sr/^{86}Sr$ ratios of the rear arc lavas imply a lesser

391 contribution of Pb and Sr from subducting sediments, and a greater contribution of these
392 elements by mafic oceanic crust. We consider how such a model may be reconciled with the K-
393 isotope data.

394 A two-stage model is presented in **Figure 6**, with parameters as described in **Table 1**. In
395 the first stage, fluids are released from the sediment and mafic oceanic crust lithologies of the
396 slab. Mixing of these fluids accounts for the isotopic composition of the lavas of the arc front.
397 The residual composition of the slab following dehydration/melting to produce the fluids is also
398 calculated. In the second stage, fluids are released from the residual sediment and residual mafic
399 oceanic crust lithologies. All parameters relating to slab dehydration/melting, including the
400 isotopic fractionation factor for $^{41}K/^{39}K$ are held constant, for both stages. The difference in the
401 sediment- and ocean-crust-derived fluids between the arc front and rear arc arises solely because
402 of the change in the composition of slab—i.e., because of the depletion of the slab by fluid loss
403 under the arc front.

404 In this simple model (**Figure 6**), an across-arc change in $\delta^{41}K$ values results from depletion
405 of the slab in heavy K. As modeled, most of the K in the lavas of both the arc front and the rear
406 arc derives from oceanic crust. This reflects the higher K/Pb ratios calculated for the oceanic-
407 crust-derived fluids as compared to the sediment-derived fluids. Thus, it is principally the loss of
408 heavy K from this reservoir—and to a lesser degree the loss of heavy K from sediment—that leads
409 to a residual slab that is relatively light. This residual slab, in turn, contributes light K to the lavas
410 of the rear arc.

411

412 4.2.4. Model 2: Control of K, Pb, and Sr by slab and mantle components

Next, we consider a model in which the mantle contributes large fractions of Pb, Sr, and K to the rear-arc (**Figure 7; Table 2**). This model rests on the assumption that the mantle is the source of unradiogenic Pb. In this model, a fluid that incorporates elements from the lower parts of the mantle wedge is included in addition to slab-derived fluids. Thus, this fluid concentrates mantle-derived Pb, Sr, and K and delivers it to part of the mantle wedge that is the source regions of the Izu lavas. The inclusion of this step, in particular, follows a model recently proposed for the Izu arc by Durkin et al. (2020). Its inclusion is motivated by the need to reconcile Pb-isotope and Pb elemental data (Straub et al., 2009; Durkin et al., 2020). This model does not account for progressive depletion of the slab.

The model is formulated as follows. First, fluids are released from the different components of slab. In addition, a fluid that has incorporated material from the mantle wedge is also released. While slab fluid loss is modeled by closed-system equilibrium (i.e., batch melting), mantle fluid loss is modeled by a 'zone-refining' process with a high solid-to-fluid ratio—namely, 200. Regarding this step, we envision that dilute aqueous fluids hydrate the mantle wedge above the slab in the forearc region. As mantle-wedge materials are dragged downward, these parcels of mantle dehydrate, releasing fluids that incorporate elements from the mantle. The composition of the metasomatic fluids that reach the Izu arc source is then a mixture of both mantle-derived and slab-derived fluids.

We also incorporate assumptions about mantle heterogeneity. A slightly more enriched radiogenic-isotope signature is assigned to the sub-rear-arc mantle. This is based on the assumption that the lower $^{143}Nd/^{144}Nd$ ratios of the rear-arc lavas are indicative of an enriched

435 mantle component (rather than a sediment component) under the rear arc. In addition, the
436 elemental composition of the sub-rear-arc mantle is inferred to be more enriched. Elemental
437 compositions of the arc-front and rear-arc mantle wedge are inferred from X/Yb vs. Nb/Yb
438 systematics, as described in the **Supplement**. These assumptions and inferences result in
439 different compositions of the mantle-derived fluids under the arc front vs. rear arc.

440 Importantly, the model is also sensitive to assumptions about the partitioning of
441 elements. Some assumptions are motivated by our aim of fitting isotopic and elemental
442 compositions of the arc lavas. In addition, we find that it is necessary that the Sr/Pb ratio of the
443 sediment-derived fluid be lower than the ratio of bulk sediment at Site 1149. Otherwise, the
444 curvature of the mixing curve in **Figure 7** will be too extreme to explain the compositions of the
445 arc lavas. Accordingly, we effectively treat the partition coefficient $\mathrm{D}_{\mathrm{Pb}}^{\mathrm{Sed/Fluid}}$ as an adjustable
446 parameter, and assign it a value of $\mathrm{D}_{\mathrm{Sr}}^{\mathrm{Sed/Fluid}}$ multiplied by a factor of 2. This value does fall
447 within the range of plausible values, given that there are large uncertainties in experimental
448 partition coefficients applicable to sediment melting (**Supplement**). In addition, we assume that
449 the fluid that incorporates material from the mantle wedge is an aqueous fluid. This has the
450 advantage of mobilizing Pb preferentially over the LREEs. Moreover, we specifically use the
451 partition coefficients for clinopyroxene/fluid and garnet/fluid from the 6 GPa and 800 C
452 experiments of Kessel et al. (2005) to model this fluid-mantle interaction. These choices lead to
453 an adequate fit for several elements (**Supplement**), but they do not resolve all problems for the
454 model. The limitations of the model are discussed later, at the end of this section.

455 The model illustrates how a signal in $\delta^{41}\mathrm{K}$ from slab-derived K is expressed in the arc front
456 but is attenuated in the rear arc. The heavy K of the slab fluid arises as a result of isotopic

457 fractionation. A fractionation factor ($\Delta_{\mathrm{slab-fluid}}$) of -0.50‰ is employed in order to generate
458 sufficiently heavy K. Mixing with mantle-derived fluids leads to lower $\delta^{41}\mathrm{K}$ values. This reflects
459 our assumption that isotopic fractionation is associated with slab dehydration and melting but
460 not mantle-fluid interaction. Accordingly, the across-arc change in $\delta^{41}\mathrm{K}$ values is partly explained
461 by a greater contribution by mantle-derived fluid in the rear arc. Note that, in addition to this
462 simple dynamic, there are also different curvatures for the mixing relationships in the $^{206}Pb/^{204}Pb$
463 — $\delta^{41}\mathrm{K}$ diagram. This reflects the different K/Pb ratios of the mixing components under the arc
464 front versus rear arc (**Figure 7**). The mixing curve for the rear arc has greater curvature. This
465 reflects the more-enriched (high K/Pb) composition inferred for the sub-rear-arc mantle. To a
466 lesser degree, it also reflects the greater contribution of sediment (low K/Pb) and lesser
467 contribution of oceanic crust (high K/Pb) to the slab-derived fluid under the rear arc. These
468 general trends illustrate how across-arc $\delta^{41}\mathrm{K}$ variations may relate to across-arc Pb-isotope
469 variations, in the context of a model where unradiogenic Pb is interpreted as deriving from the
470 mantle wedge.
471
472 Limitations of Model 2
473
474 We conclude by noting that the validity of this model depends mostly on factors other than how
475 well it can explain the K-isotope data. One challenge is whether a fluid interacting with the
476 mantle can acquire elemental patterns that are consistent with the elemental patterns observed
477 in the Izu lavas. In particular, in order for this model to be successful, the fluid must incorporate
478 Pb, Sr, and K (with similar efficiency) from the mantle while not incorporating too much LREEs or

Nb or Ta. Many partition coefficients for fluid-mantle or melt-mantle interaction do not meet these criteria. The set of coefficients we have used results in an adequate fit for several elements, but does not reproduce the low Nb or La abundances that are needed (**Supplement**). The mismatches for these elements is usually less than a factor of 2. Perhaps there is enough uncertainty regarding partition coefficients, so that this does not preclude the viability of the model. Another challenge is whether a fluid can transfer sufficient amounts of mantle-derived material without also transporting excessive amounts of H_2O. Our modeling requires about 5% metasomatic fluid to be added to the parts of the mantle wedge that are the arc source regions. If this metasomatic fluid is highly H_2O-rich—e.g., greater than 50% H_2O, which would be consistent with our choice of partition coefficients—then this may produce unrealistically high H_2O contents in the primary arc lavas. Thus, the model as formulated would likely require some mechanism to lose H_2O from the metasomatic fluids and/or primary magmas.

5. Conclusions

(1) The lavas of the Izu arc have high $\delta^{41}K$ values relative to our current best estimates for the upper mantle, sediments, and ocean crust. We infer that heavy K is mobilized preferentially by fluids during slab dehydration.

(2) A decrease in $\delta^{41}K$ values is observed from arc front to rear arc. Arc front and rear arc lavas are typically heavier than the upper mantle by about 0.22‰ and 0.08‰, respectively. This shift

500 may reflect a progressive depletion of the slab in heavy K, resulting in the release of progressively
501 lighter K as the slab descends to greater depths.
502
503 (3) Lead and Sr isotope relationships have been interpreted in fundamentally different ways in
504 the setting of the Izu arc. If unradiogenic Pb is derived from the mantle (as suggested by some
505 lines of evidence), then it appears that fluids must efficiently scavenge Pb and presumably other
506 fluid-mobile elements from the mantle wedge. In this scenario, the across-arc decrease in $\delta^{41}\mathrm{K}$
507 values may also be related to a greater contribution of K from the mantle wedge to the rear-arc
508 lavas.
509
510 (4) Potassium isotopes may be useful in tracking the depletion of subducting slabs in K and other
511 elements. Since K is hosted in hydrous and LILE-bearing phases, such as phengite or phlogopite,
512 K-isotope variations in arc lavas may contribute to understanding the fate of H_2O and LILEs in
513 subduction zones.
514
515 (5) To the extent that preferential loss of heavy K by the slab is common in subduction zones, it
516 will be the case that heavier K will be added to arc and continental crust whereas lighter K will be
517 added to the mantle. Future work can assess whether a difference in K-isotope compositions
518 between continental crust and mantle can be resolved.
519

(6) Very large $\delta^{41}K$ variations among a subset of samples are not well-understood. Provisionally, these variations are attributed to processes that occur at shallow or crustal depths that may conceivably mobilize K to a significant degree.

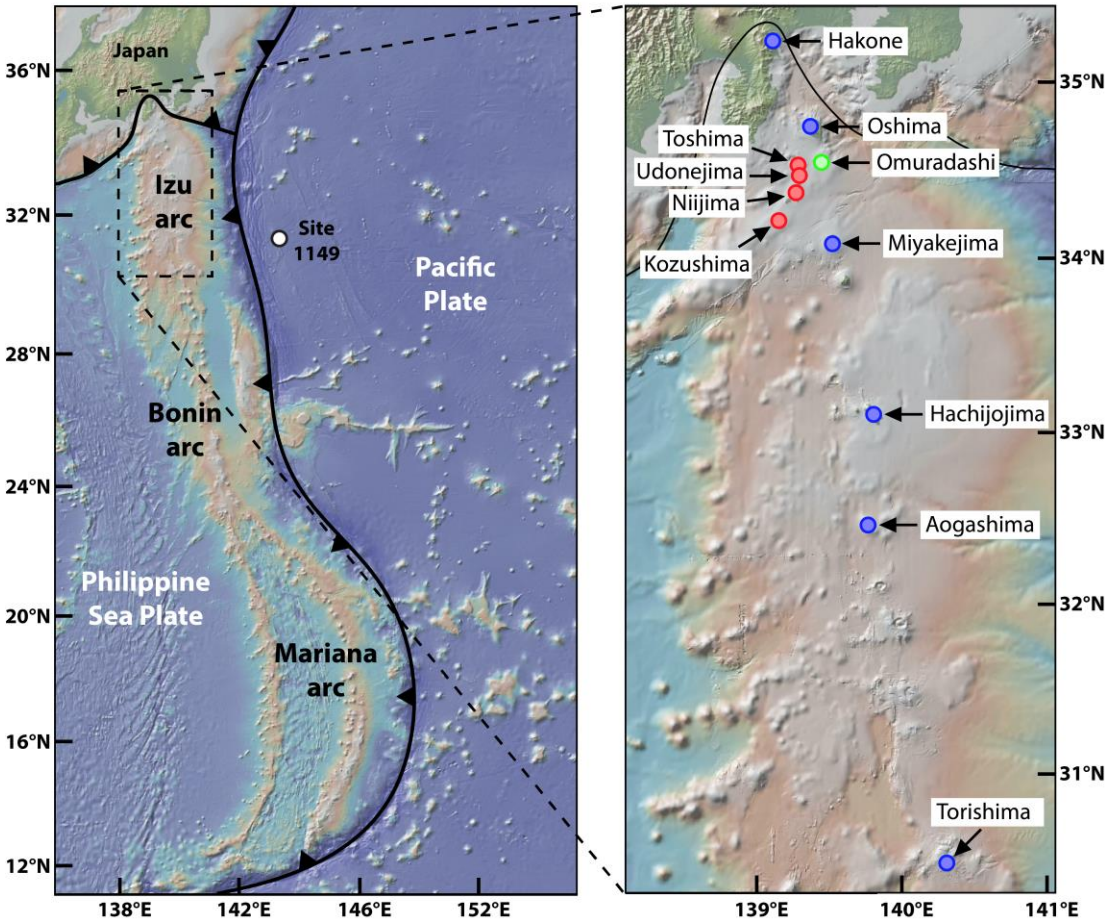

Figure 1. (Left) Overview of the Izu-Bonin-Mariana arc, and location of IODP Site 1149. (Right) Volcanos of the Izu arc from which we obtained samples. Arc front volcanic islands and Hakone volcano denoted by blue markers, rear-arc volcanic islands by red markers, and the submerged caldera Omuradashi by a green marker. Bathymetric data from Ryan et al. (2009), plotted with GeoMapApp software (www.geomapapp.org).

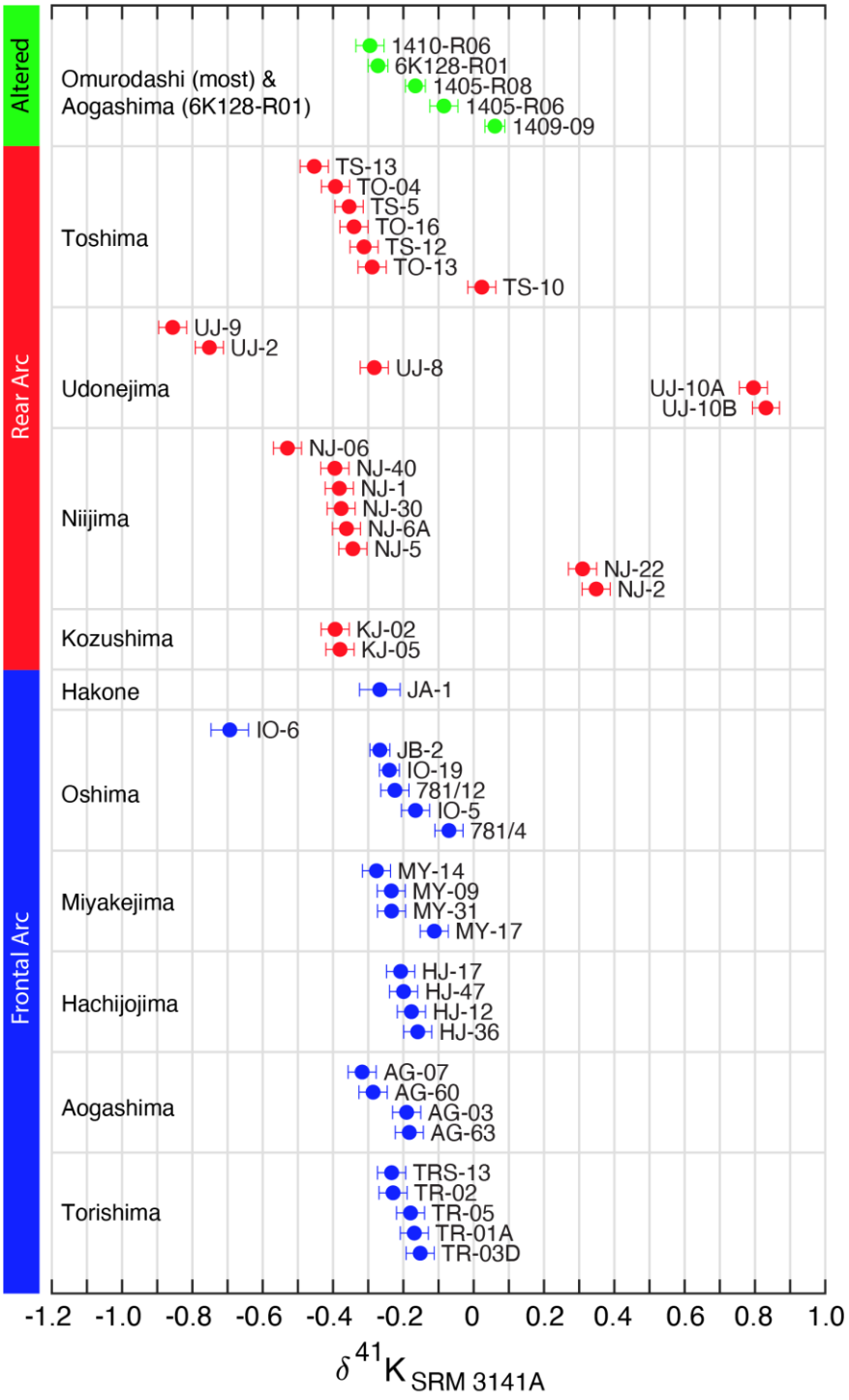

Figure 2. Graphical summary of $\delta^{41}K$ values in all samples reported in this study. Within the arc front and rear arc groups, volcanic islands (and Hakone volcano) are ordered vertically according to their latitude. Note that the altered samples appear to have more variable $\delta^{41}K$ values, extending to higher values, in comparison to unaltered arc front samples.

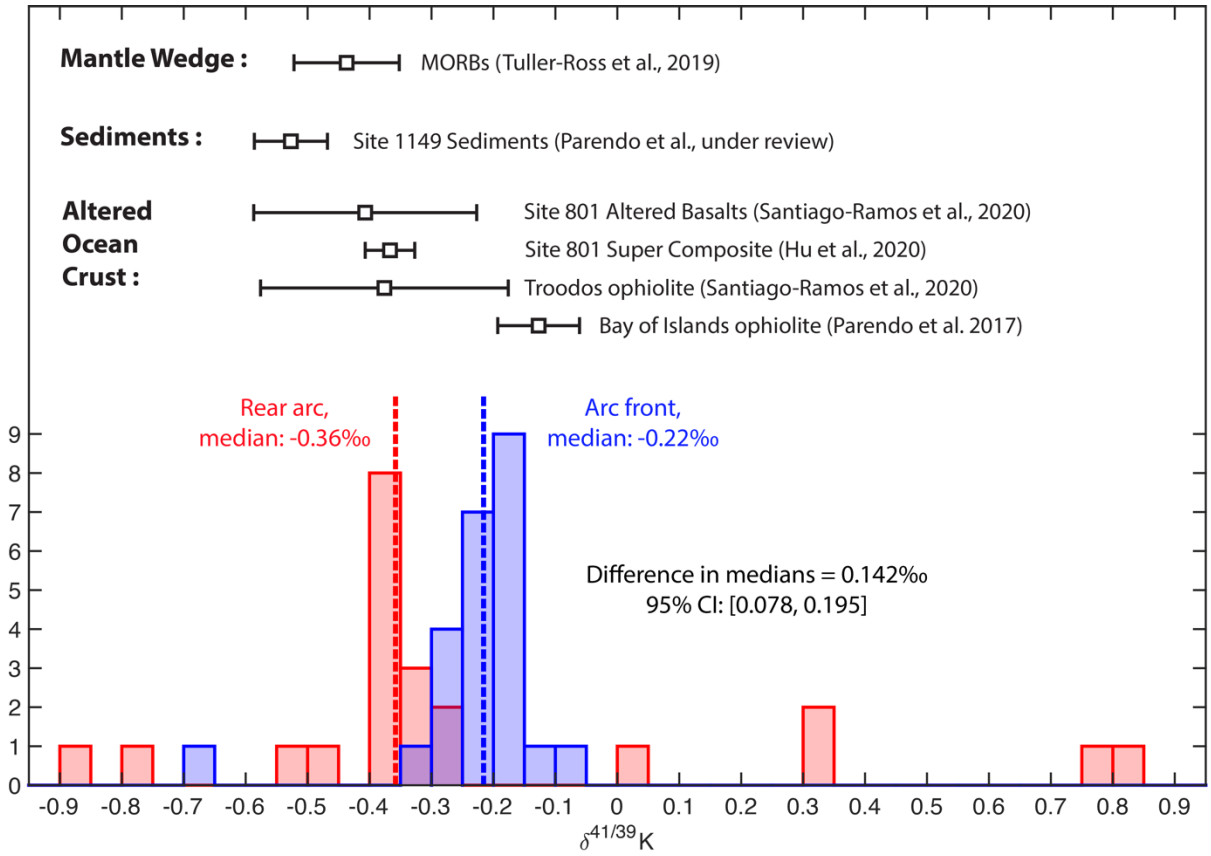

Figure 3. Distributions of δ^{41}K values for arc front and rear arc samples. Median values are indicated by dashed vertical lines. The difference between the medians is 0.14‰, with a 95% confidence interval [0.078 to 0.195‰] calculated by a bootstrapping approach. Literature data bearing on the compositions of the mantle wedge, sediments, and altered oceanic crust are summarized: Markers indicate mean values, and horizontal bars indicate $\pm$ one standard deviation.

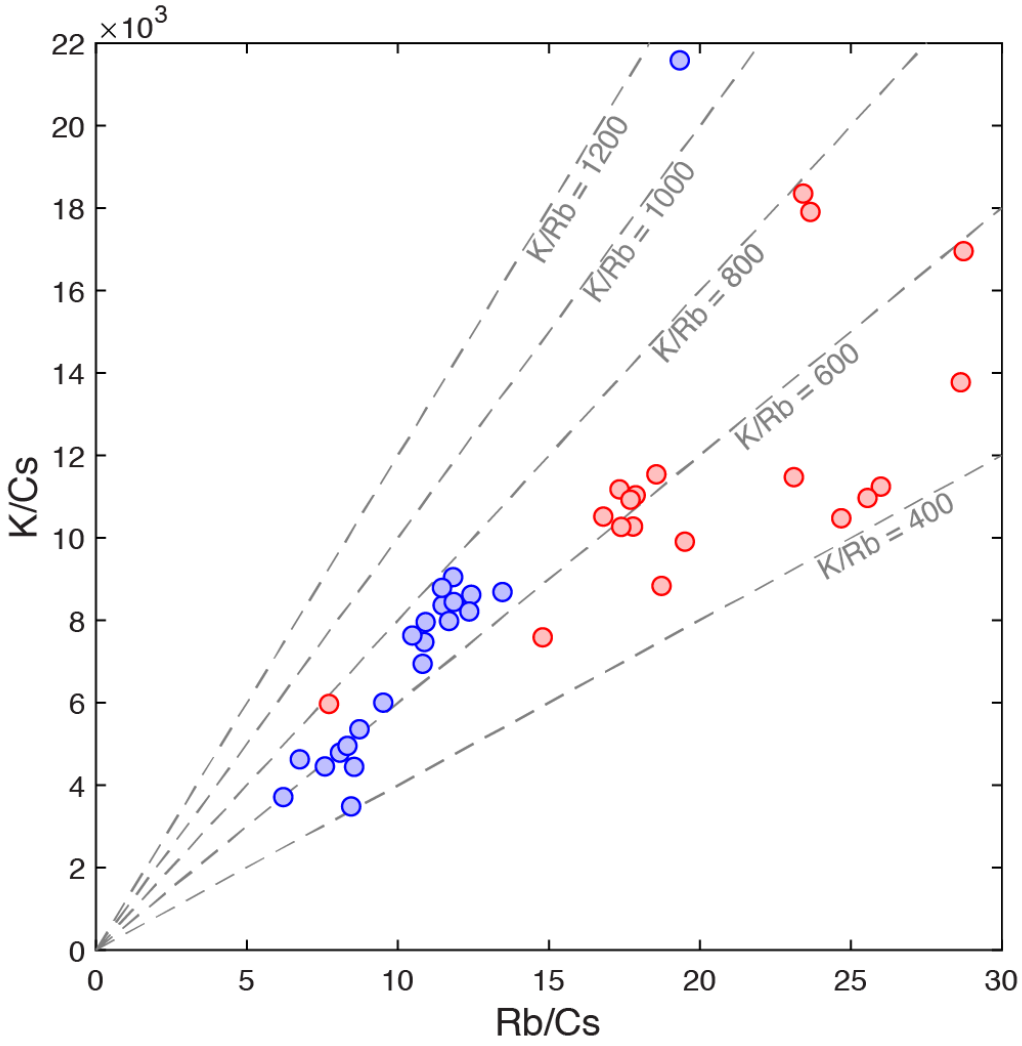

Figure 4. Alkali element (K, Rb, Cs) ratios of the Izu arc lavas. Ratios of K/Cs and Rb/Cs are generally higher in the rear arc lavas (red) than in the arc front lavas (blue). The decrease in $\delta^{41}K$ values from the arc front to rear arc is consistent with the across-arc increase in K/Cs and Rb/Cs ratios, in that they both support progressive breakdown of phengite with depth in the subduction zone.

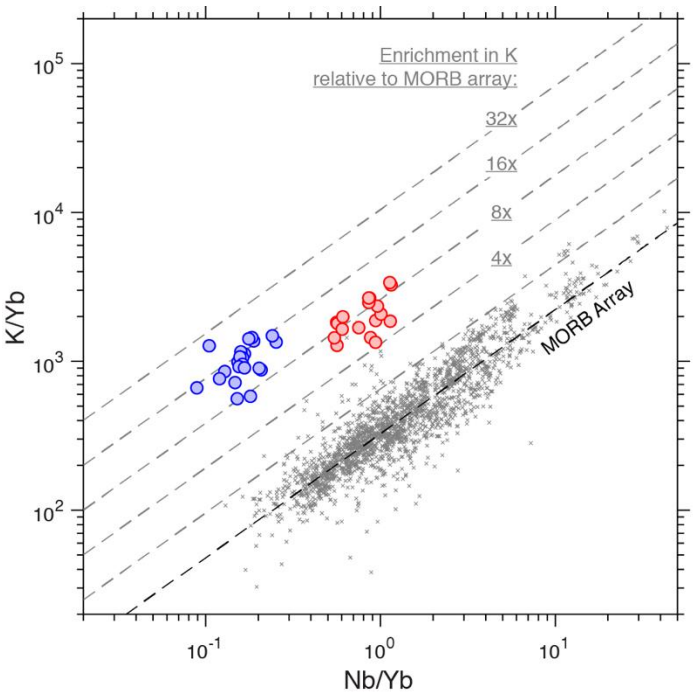

584

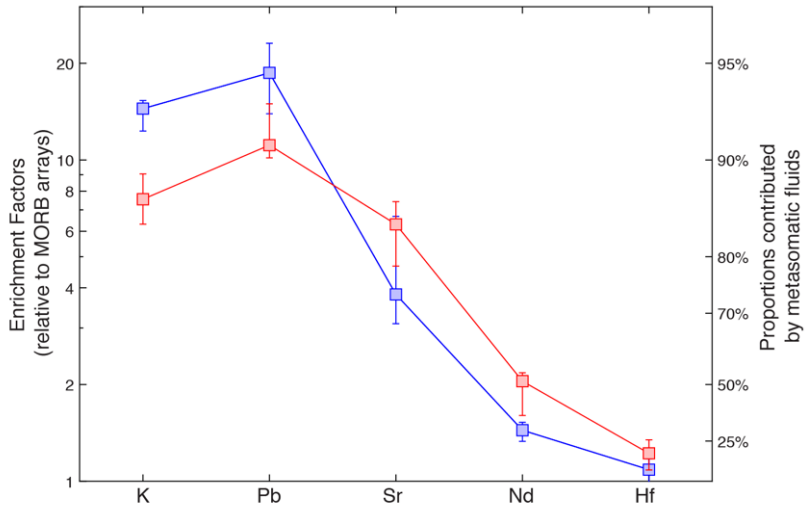

585

586 **Figure 5.** (a-Top) Potassium enrichment as quantified by K/Yb – Nb/Yb systematics, after Pearce
587 (1982) and Pearce and Stern (2006). Global MORB data from the compilation of Gale et al. (2013).
588 Black dashed line is regressed through MORB data points. The grey dashed lines are contours
589 that correspond to the enrichment factors of K/Yb relative to the MORB array. (b-Bottom)
590 Enrichments of K, Pb, Sr, Nd, and Hf as quantified by X/Yb – Nb/Yb systematics, where X is K, Pb,
591 Sr, Nd, or Hf. Proportions of each element contributed by metasomatic fluids is also indicated.
592 For each element, markers are based on median values, and bars correspond to 25th and 75th
593 percentile values. Bars are not intended to represent all sources of uncertainty.
594

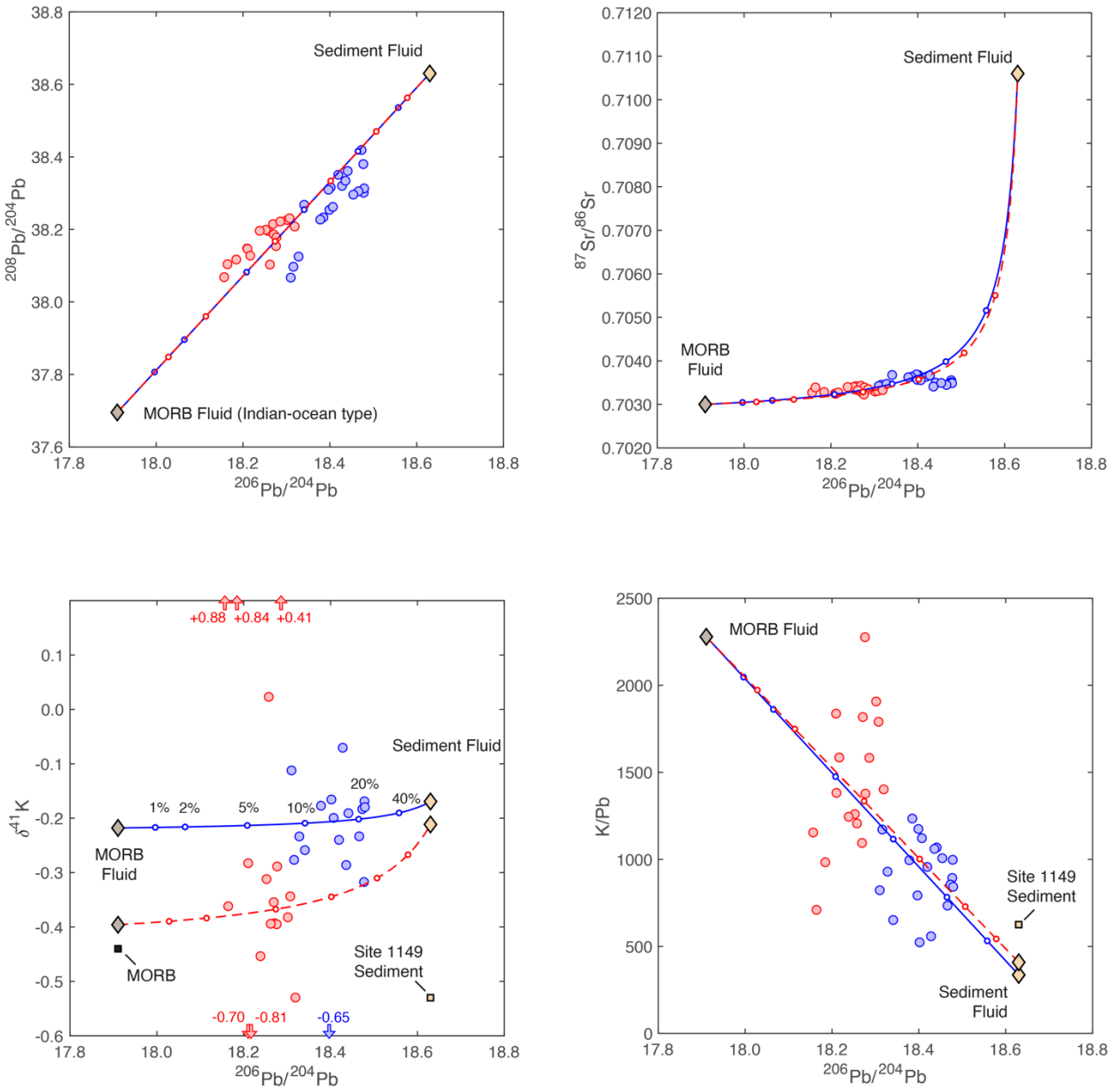

595

596 **Figure 6.** Relationships from Model 1: Control of K, Pb, and Sr by slab components. The
597 compositions of the Izu lavas are modelled as mixtures of sediment and MORB (lower ocean
598 crust) fluids. The MORB component is assumed to be negligibly affected by seafloor
599 hydrothermal alteration. A fractionation factor ($\Delta_{solid-fluid}$ = -0.40‰) is assumed. Depletion of
600 the slab by fluid loss under the arc front modifies the composition of the slab, resulting in
601 different fluid compositions being released under the rear arc. Model 1 parameters are provided
602 in Table 1.
603
604
605
606

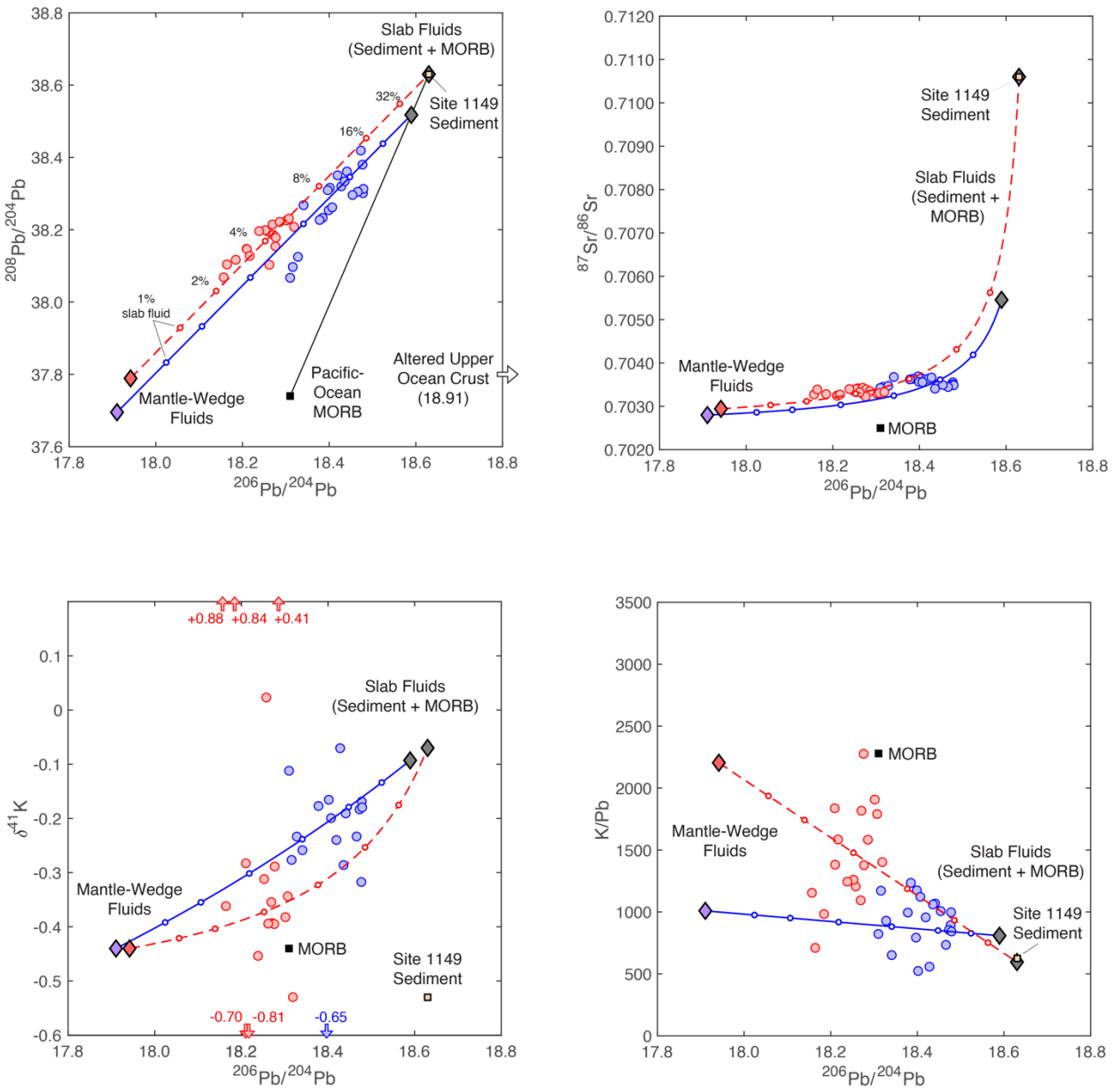

607

608 **Figure 7.** Relationships from Model 2: Control of K, Pb, and Sr by slab and mantle components.
609 The compositions of the Izu lavas are modelled as mixtures of slab-derived (sediment- and MORB-
610 derived) fluids and mantle-wedge-derived fluids. Depletion of the slab by progressive fluid loss
611 is neglected in this model. A fractionation factor ($\Delta_{\text{solid}-\text{fluid}}$ = -0.50‰) is assumed. In the arc
612 front, the slab-derived fluid includes sediment and MORB components. In the rear arc, the slab-
613 derived-fluid includes only sediment components. Mantle-wedge fluids vary in composition as a
614 result of inferred compositional heterogeneity in the mantle wedge. Model 2 parameters are
615 provided in Table 2.
616
617
618

Table 1

Parameters used for modeling in Figure 6.

	Sed. (1)	Sed. Fluid (2)	MORB, Indian-Ocean-Type (3)	MORB Fluid (4)	Residual Sed. (5)	Residual-Sed. Fluid (6)	Residual MORB (7)	Residual-MORB Fluid (8)
Pb	15.4	122	0.51	9.1	12.7	100	0.29	5
Sr	136	1075	128	1807	112	884	85	1199
K	9630.3	40929	1162.3	20681	8907	40929	662	11776
$^{206}Pb/^{204}Pb$	18.63	18.63	17.91	17.91	18.63	18.63	17.9105	17.91
$^{208}Pb/^{204}Pb$	38.63	38.63	37.70	37.70	38.63	38.63	37.6951	37.70
$^{87}Sr/^{86}Sr$	0.7106	0.7106	0.7030	0.7030	0.7106	0.7106	0.7030	0.7030
$\delta^{41}K$	-0.53	-0.17	-0.44	-0.22	-0.57	-0.21	-0.62	-0.40

Table 1 Caption

(1) Sediment elemental composition is Site 1149 weighted average from Plank et al. (2007). Radiogenic isotope compositions from averaging of data from Hauff et al. (2003), Chavagnac et al. (2008), and Scudder et al. (2014): see supplement. Potassium-isotope composition from a Site 1149 average (Parendo et al., under review): data included in supplement.

(2) Sediment-fluid composition is calculated by batch melting with melt fraction of 2.5%. Partition coefficient for Sr ($D_{Sr}^{solid/liquid}$) from experiment C-1699 (3.5 GPa, 900 C) of Hermann and Rubatto (2009). $D_{Pb}^{s/l}$ is assumed equal to $D_{Sr}^{s/l}$. Potassium content of fluid is buffered by phengite: a saturation concentration of 4.9% is used (experiment C-1699; Hermann and Rubatto, 2009). A fractionation factor ($\alpha^{s/l}$) for $^{41}K/^{39}K$ of 0.9996 is assumed.

(3) MORB elemental composition is N-MORB of Gale et al. (2013). Pb-isotope composition is estimated from average of back-arc-basin basalt data of Hickey-Vargas (1991) and Straub et al. (2010). Sr-isotope composition is adjusted to a slightly higher value (by about ~0.0002) than an average of data from Hickey-Vargas (1991) and Straub et al. (2010), following assumption of Straub et al. (2010) that Sr may be affected slightly by seawater alteration; This value (0.7030) is also the same as the median of Indian-Ocean MORB samples from the compilation of Gale et al. (2010). Potassium-isotope composition from Tuller-Ross et al. (2019).

(4) MORB-fluid composition is calculated by batch melting (dehydration) with melt (fluid) fraction of 2.5%. Partition coefficients $D_{Pb}^{s/l}$ and $D_{Sr}^{s/l}$ from 4 GPa and 900 C experiment of Kessel et al. (2005). $D_{K}^{s/l}$ is assumed equal to $D_{Pb}^{s/l}$. A fractionation factor ($\alpha^{s/l}$) for $^{41}K/^{39}K$ of 0.9996 is assumed.

(5) Residual sediment is composition of sediment following loss of material according to melting described in footnote (2).

(6) Residual-sediment fluid is composition of fluid produced by melting using the same parameters as in footnote (3).

(7) Residual MORB is composition of sediment following loss of material according to melting described in footnote (4).

(8) Residual-MORB fluid is composition of fluid produced by melting (dehydration) using the same parameters as in footnote (5).

Table 2

Parameters used for modeling in Figure 7.

	Sed. (1)	Sed. Fluid (2)	MORB, Pacific-Type (3)	MORB Fluid (4)	Arc-Front Slab Fluid (5)	Rear-Arc Slab Fluid (6)	Arc-Front Mantle (7)	Arc-Front Mantle Fluid (8)	Rear-Arc Mantle (7)	Rear-Arc Mantle Fluid (8)
Pb	15.4	69	0.51	9.9	39	69	0.016	2.0	0.027	3.5
Sr	136	1114	128	1938	1526	1114	4.9	656	7.3	973
K	9630.3	40929	1162	22630	31780	40929	16	1994	61	7666
$^{206}Pb/^{204}Pb$	18.63	18.63	18.31	18.31	18.59	18.63	17.91	17.91	17.94	17.94
$^{208}Pb/^{204}Pb$	38.63	38.63	37.74	37.74	38.52	38.63	37.70	37.70	37.79	37.79
$^{87}Sr/^{86}Sr$	0.7106	0.7106	0.7025	0.7025	0.7055	0.7106	0.7028	0.7028	0.7029	0.7029
$\delta^{41}K$	-0.53	-0.07	-0.44	-0.13	-0.09	-0.07	-0.44	-0.44	-0.44	-0.44

Table 2 Caption

(1) Sediment elemental composition is Site 1149 weighted average from Plank et al. (2007). Radiogenic isotope compositions from averaging of data from Hauff et al. (2003), Chavagnac et al. (2008), and Scudder et al. (2014): see supplement. Potassium-isotope composition from a Site 1149 average (Parendo et al., under review): data included in supplement.

(2) Sediment-fluid composition is calculated by batch melting with melt fraction of 2.0%. Partition coefficient for Sr ($D_{Sr}^{solid/liquid}$) from experiment C-1699 (3.5 GPa, 900 C) of Hermann and Rubatto (2009). $D_{Pb}^{s/l}$ is assumed equal to (2 * $D_{Sr}^{s/l}$). Potassium content of fluid is buffered by phengite: a saturation concentration of 4.9% is used (experiment C-1699; Hermann and Rubatto, 2009). A fractionation factor ($\alpha^{s/l}$) for $^{41}K/^{39}K$ of 0.9995 is assumed.

(3) MORB elemental composition is N-MORB of Gale et al. (2013). Radiogenic-isotope composition is average of individual Pacific MORB samples from compilation of Gale et al. (2013). Potassium-isotope composition from Tuller-Ross et al. (2019).

(4) MORB-fluid composition is calculated by batch melting (dehydration) with melt (fluid) fraction of 2.5%. Partition coefficients $D_{Pb}^{s/l}$ and $D_{Sr}^{s/l}$ from 4 GPa and 900 C experiment of Kessel et al. (2005). $D_{K}^{s/l}$ is assumed equal to $D_{Pb}^{s/l}$. A fractionation factor ($\alpha^{s/l}$) for $^{41}K/^{39}K$ of 0.9995 is assumed.

(5) Arc-front slab fluid is a mixture of 50% sediment fluid and 50% MORB fluid.

(6) Rear-arc slab fluid is identical to the sediment fluid.

(7) Elemental compositions of mantle wedge under arc front and rear arc obtained are inferred on the basis of Nb/Yb ratios, X/Yb — Nb/Yb systematics, and assumptions of extents of melting of the mantle wedge of 28% and 16% below the arc front and rear arc., respectively See supplement for full explanation. Strontium and Pb values under arc front are average values of BABBs of the Shikoku Basin (Hickey-Vargas, 1991; Straub et al., 2010), and values under rear arc are midway between values for BABBs and values for the Kinan Seamount Chain (KSC; Ishizuka et al., 2009): This selection of radiogenic-isotope compositions is intended also to consistent with $^{143}Nd/^{144}Nd$ variation across the arc, under the assumption that $^{143}Nd/^{144}Nd$ variation reflects mantle heterogeneity. Potassium-isotope composition is same as for MORB.

(8) Mantle-fluid compositions for sub-arc-front and sub-rear-arc calculated by 'zone-refining' interaction of an initially pure fluid with sub-arc-front and sub-rear-arc mantle wedge at a solid-to-fluid ratio of 200: This is similar in effect to producing a fluid by batch melting at a low extent of melting, i.e., about 0.5%. Partition coefficients for Pb and Sr from 800 C and 6 GPa experiment of Kessel et al. (2005), and assuming a mantle wedge mineralogy that includes 5% garnet and 5% clinopyroxene. Other minerals are assumed to retain negligible amounts of trace elements. $D_{K}^{s/l}$ is assumed equal to $D_{Pb}^{s/l}$. A fractionation factor ($\alpha^{s/l}$) for $^{41}K/^{39}K$ of unity is assumed.

6. References

Parendo, C., Jacobsen, S.B., Plank, T., (submitted) Controls on the K-isotope compositions of marine sediments and ocean-floor basalts adjacent to the Izu-Bonin Trench and Nankai Trough.

Ayers, J. (1998) Trace element modeling of aqueous fluid–peridotite interaction in the mantle wedge of subduction zones. Contributions to Mineralogy and Petrology 132, 390-404.

Durkin, K., Castillo, P.R., Straub, S.M., Abe, N., Tamura, Y. and Yan, Q. (2020) An origin of the along-arc compositional variation in the Izu-Bonin arc system. Geoscience Frontiers 11, 1621-1634.

Freymuth, H., Andersen, M. B., & Elliott, T. (2019). Uranium isotope fractionation during slab dehydration beneath the Izu arc. *Earth and Planetary Science Letters*, *522*, 244-254.

Gale, A., Dalton, C.A., Langmuir, C.H., Su, Y. and Schilling, J.G. (2013) The mean composition of ocean ridge basalts. Geochemistry, Geophysics, Geosystems 14, 489-518.

Hauff, F., Hoernle, K. and Schmidt, A. (2003) Sr-Nd-Pb composition of Mesozoic Pacific oceanic crust (Site 1149 and 801, ODP Leg 185): Implications for alteration of ocean crust and the input into the Izu-Bonin-Mariana subduction system. Geochemistry, Geophysics, Geosystems 4.

Hermann, J. and Rubatto, D. (2009) Accessory phase control on the trace element signature of sediment melts in subduction zones. Chemical Geology 265, 512-526.

Hermann, J., Spandler, C., Hack, A. and Korsakov, A.V. (2006) Aqueous fluids and hydrous melts in high-pressure and ultra-high pressure rocks: implications for element transfer in subduction zones. Lithos 92, 399-417.

Hermann, J. and Spandler, C.J. (2008) Sediment Melts at Sub-arc Depths: an Experimental Study. Journal of Petrology 49, 717-740.

Hickey-Vargas, R. (1991) Isotope characteristics of submarine lavas from the Philippine Sea: implications for the origin of arc and basin magmas of the Philippine tectonic plate. Earth and Planetary Science Letters 107, 290-304.

Hickey-Vargas, R. (1998) Origin of the Indian Ocean-type isotopic signature in basalts from Philippine Sea plate spreading centers: An assessment of local versus large-scale processes. Journal of Geophysical Research: Solid Earth 103, 20963-20979.

Hochstaedter, A., Gill, J., Peters, R., Broughton, P., Holden, P. and Taylor, B. (2001) Across-arc geochemical trends in the Izu-Bonin arc: Contributions from the subducting slab. Geochemistry, Geophysics, Geosystems 2.

Hu, Y., Teng, F.-Z. and Chauvel, C. (2021) Potassium isotopic evidence for sedimentary input to the mantle source of Lesser Antilles lavas. Geochimica et Cosmochimica Acta 295, 98-111.

727 Hu, Y., Teng, F.-Z., Plank, T. and Chauvel, C. (2020) Potassium isotopic heterogeneity in subducting
728 oceanic plates. Science Advances 6, eabb2472.

729 Huang, T.-Y., Teng, F.-Z., Rudnick, R.L., Chen, X.-Y., Hu, Y., Liu, Y.-S. and Wu, F.-Y. (2019)
730 Heterogeneous potassium isotopic composition of the upper continental crust. Geochimica et
731 Cosmochimica Acta.

732 Ishizuka, O., Taylor, R.N., Milton, J.A., Nesbitt, R.W., Yuasa, M. and Sakamoto, I. (2006) Variation
733 in the mantle sources of the northern Izu arc with time and space—Constraints from high-
734 precision Pb isotopes. Journal of Volcanology and Geothermal Research 156, 266-290.

735 Ishizuka, O., Yuasa, M., Taylor, R.N. and Sakamoto, I. (2009) Two contrasting magmatic types
736 coexist after the cessation of back-arc spreading. Chemical Geology 266, 274-296.

737 Kelley, K.A., Plank, T., Ludden, J. and Staudigel, H. (2003) Composition of altered oceanic crust at
738 ODP Sites 801 and 1149. Geochemistry, Geophysics, Geosystems 4.

739 Keppler, H. (2017) Fluids and trace element transport in subduction zones. American Mineralogist
740 102, 5-20.

741 Kessel, R., Schmidt, M.W., Ulmer, P. and Pettke, T. (2005) Trace element signature of subduction-
742 zone fluids, melts and supercritical liquids at 120–180 km depth. Nature 437, 724-727.

743 Kimura, J.I., Kent, A.J., Rowe, M.C., Katakuse, M., Nakano, F., Hacker, B.R., van Keken, P.E.,
744 Kawabata, H. and Stern, R.J. (2010) Origin of cross-chain geochemical variation in Quaternary
745 lavas from the northern Izu arc: using a quantitative mass balance approach to identify mantle
746 sources and mantle wedge processes. Geochemistry, Geophysics, Geosystems 11.

747 Li, Y., Wang, W., Wu, Z. and Huang, S. (2019) First-principles investigation of equilibrium K isotope
748 fractionation among K-bearing minerals. Geochimica et Cosmochimica Acta 264, 30-42.

749 Liu, H., Wang, K., Sun, W.-D., Xiao, Y., Xue, Y.-Y. and Tuller-Ross, B. (2020) Extremely light K in
750 subducted low-T altered oceanic crust: Implications for K recycling in subduction zone.
751 Geochimica et Cosmochimica Acta 277, 206-223.

752 Mazza, S. E., Stracke, A., Gill, J. B., Kimura, J. I., & Kleine, T. (2020). Tracing dehydration and
753 melting of the subducted slab with tungsten isotopes in arc lavas. *Earth and Planetary Science*
754 *Letters*, *530*, 115942.
755
756 Melzer, S. and Wunder, B. (2000) Island-arc basalt alkali ratios: Constraints from phengite-fluid
757 partitioning experiments. Geology 28, 583-586.

758 Parendo, C.A., Jacobsen, S.B. and Wang, K. (2017) K isotopes as a tracer of seafloor hydrothermal
759 alteration. Proceedings of the National Academy of Sciences, 201609228.

760 Pearce, J.A. (1982) Trace element characteristics of lavas from destructive plate boundaries.
761 Andesites 8, 525-548.

762 Pearce, J.A. and Stern, R.J. (2006) Origin of back-arc basin magmas: trace element and isotope
763 perspectives. Geophysical Monograph-American Geophysical Union 166, 63.

764 Pirard, C., & Hermann, J. (2015). Focused fluid transfer through the mantle above subduction
765 zones. *Geology*, *43*(10), 915-918.
766
767 Plank, T., Kelley, K.A., Murray, R.W. and Stern, L.Q. (2007) Chemical composition of sediments
768 subducting at the Izu-Bonin trench. Geochemistry, Geophysics, Geosystems 8.

769 Ryan, W.B., Carbotte, S.M., Coplan, J.O., O'Hara, S., Melkonian, A., Arko, R., Weissel, R.A., Ferrini,
770 V., Goodwillie, A. and Nitsche, F. (2009) Global multi-resolution topography synthesis.
771 Geochemistry, Geophysics, Geosystems 10.

772 Salters, V.J. and Stracke, A. (2004) Composition of the depleted mantle. Geochemistry,
773 Geophysics, Geosystems 5.

774 Santiago Ramos, D.P., Coogan, L.A., Murphy, J.G. and Higgins, J.A. (2020) Low-temperature
775 oceanic crust alteration and the isotopic budgets of potassium and magnesium in seawater. Earth
776 and Planetary Science Letters 541, 116290.

777 Schmidt, M.W., Vielzeuf, D. and Auzanneau, E. (2004) Melting and dissolution of subducting crust
778 at high pressures: the key role of white mica. Earth and Planetary Science Letters 228, 65-84.

779 Sekine, T. and Wyllie, P.J. (1982) Phase relationships in the system KAlSiO 4-Mg 2 SiO 4-SiO 2-H 2
780 O as a model for hybridization between hydrous siliceous melts and peridotite. Contributions to
781 Mineralogy and Petrology 79, 368-374.

782 Spandler, C., & Hermann, J. (2006). High-pressure veins in eclogite from New Caledonia and
783 their significance for fluid migration in subduction zones. *Lithos*, *89*(1-2), 135-15
784
785 Spandler, C. and Pirard, C. (2013) Element recycling from subducting slabs to arc crust: A review.
786 Lithos 170-171, 208-223.

787 Straub, S.M., Goldstein, S.L., Class, C. and Schmidt, A. (2009) Mid-ocean-ridge basalt of Indian
788 type in the northwest Pacific Ocean basin. Nature Geoscience 2, 286-289.

789 Straub, S.M., Goldstein, S.L., Class, C., Schmidt, A. and Gomez-Tuena, A. (2010) Slab and mantle
790 controls on the Sr–Nd–Pb–Hf isotope evolution of the post 42 Ma Izu–Bonin volcanic arc. Journal
791 of Petrology 51, 993-1026.

792 Syracuse, E.M., van Keken, P.E. and Abers, G.A. (2010) The global range of subduction zone
793 thermal models. Physics of the Earth and Planetary Interiors 183, 73-90.

794 Tamura, Y., Tani, K., Chang, Q., Shukuno, H., Kawabata, H., Ishizuka, O. and Fiske, R.S. (2007) Wet
795 and dry basalt magma evolution at Torishima Volcano, Izu–Bonin Arc, Japan: the possible role of
796 phengite in the downgoing Slab. Journal of Petrology 48, 1999-2031.

797 Taylor, R.N. and Nesbitt, R.W. (1998) Isotopic characteristics of subduction fluids in an intra-
798 oceanic setting, Izu–Bonin Arc, Japan. Earth and Planetary Science Letters 164, 79-98.

799 Tollstrup, D., Gill, J., Kent, A., Prinkey, D., Williams, R., Tamura, Y. and Ishizuka, O. (2010) Across-
800 arc geochemical trends in the Izu-Bonin arc: Contributions from the subducting slab, revisited.
801 Geochemistry, Geophysics, Geosystems 11.

802 Tuller-Ross, B., Marty, B., Chen, H., Kelley, K.A., Lee, H. and Wang, K. (2019a) Potassium isotope
803 systematics of oceanic basalts. Geochimica et Cosmochimica Acta 259, 144-154.

804 Villalobos-Orchard, J., Freymuth, H., O'Driscoll, B., Elliott, T., Williams, H., Casalini, M., &
805 Willbold, M. (2020). Molybdenum isotope ratios in Izu arc basalts: The control of subduction
806 zone fluids on compositional variations in arc volcanic systems. *Geochimica et Cosmochimica*
807 *Acta*, *288*, 68-82.
808
809 Zeng, H., Rozsa, V.F., Nie, N.X., Zhang, Z., Pham, T.A., Galli, G. and Dauphas, N. (2019) Ab Initio
810 calculation of equilibrium isotopic fractionations of potassium and rubidium in minerals and
811 water. ACS Earth and Space Chemistry 3, 2601-2612.
812

Acknowledgements:

We thank Michail I. Pataev for operating the electron-microprobe and assisting in the interpretation of petrographic images, and for helpful discussions. This work was funded by National Science Foundation Grant EAR-1144727 and NASA Emerging Worlds Program Grant 80NSSC20K0346.

Supplementary Information

Section 1:

Discussion of extreme K-isotope variations in certain samples

The subset of highly variable $\delta^{41}K$ values within our dataset requires a separate explanation. Since many processes occurring in the slab or mantle wedge are expected to entail mixing or homogenization, it is probable that these highly large variations originated after many of these processes. Thus, we focus on processes that occur at relatively shallow depths and at the Earth's surface, such as magmatic differentiation, exsolution of fluids, and secondary alteration.

Secondary alteration remains a possibility; however, petrographic evidence and other considerations suggest that it is not the responsible mechanism. To look for signs of alteration, we examined sample NJ-22, a significant $\delta^{41}K$ outlier, under petrographic microscope and by electron-microprobe. We observed that the bulk of K in this sample is hosted overwhelmingly in glassy matrix and that the glass shows no clear signs of degradation or conversion to secondary phases (**Supplement**). To check for heterogeneity, we also dissolved and analyzed two separate chips of sample NJ-22, in addition to the initial powder. The $\delta^{41}K$ values of the three pieces of NJ-22 yielded values of 0.25, 0.32, and 0.36: This range is greater than our estimated analytical reproducibility but is smaller than the gap between NJ-22 and most rear-arc samples. Large variability among different pieces of NJ-22 would probably indicate alteration, whereas the relatively narrow range of $\delta^{41}K$ values here does not provide clear evidence one way or the other. Finally, we note that we analyzed five visibly altered samples, mostly from the submarine caldera Omuradashi. Among these samples, we did not observe any extreme variations in $\delta^{41}K$ values. This provides additional evidence against alteration of glass to secondary phases—or assimilation of such material—as an explanation for the highly variable $\delta^{41}K$ values in arc front and rear arc. Based primarily on the petrographic observations, we conclude that secondary alteration is not the cause of extreme $\delta^{41}K$ variability, unless the K of the volcanic glasses can be affected dramatically without visible changes to the glass.

Fractional crystallization can be ruled out as an explanation. Potassium in the mafic and andesitic samples, in which the extreme $\delta^{41}K$ values are found, is resides overwhelmingly in the glassy matrix, since there are no significant K-bearing mineral phases in these volcanic rocks: Without K in a mineral phase, there is no mechanism by which fractional crystallization can drive $\delta^{41}K$ variations in the lavas. Moreover, the rhyolite samples in our dataset (NJ-30, NJ-40, KZ-02, KZ-05) have normal, minimally variable K-isotope compositions, supporting the conclusion that fractional crystallization has a negligible impact on $\delta^{41}K$ values. These findings are consistent with the results of Tuller-Ross et al. (2019b), who reported a lack of significant variation in $\delta^{41}K$ values among variably evolved volcanics that lack a K-bearing mineral phase, from Hekla volcano, Iceland.

Certain other magmatic processes, such as fluid exsolution or wallrock assimilation, have the potential to transfer significant amounts of K to or from magmatic systems, so these may be viable mechanisms to produce the extreme $\delta^{41}K$ values. Here, we focus primarily on the process of fluid exsolution, though it seems probable that, ultimately, both export of material by exsolved

fluids and an assimilative process may be required to fully explain the data. As magmas rise, the drop in pressure reduces the solubility of H_2O and other volatiles in the magmas, such that exsolution of aqueous solutions or vapors is expected to occur. Additionally, fluids exsolved from magmas may, in some instances, possess high solute contents, with higher K concentrations in the aqueous-solution phase than in the melt phase (Zajacz et al., 2008). Thus, we may expect exsolving fluids to significantly mobilize K in magmatic systems under certain conditions. Moreover, there is petrographic evidence to substantiate that solute-rich fluids were exsolved from the melt corresponding to sample NJ-22. Photomicrographs show that vesicles in sample NJ-22 have ingrowing euhedral phenocrysts of phases including Na-feldspar and pyroxene (**Supplement: Figures S3-S6**). This indicates that these silicate minerals were precipitated from aqueous fluids that had separated from the melt, and that the fluids were solute-rich. While the K contents of the fluids are not known, it is possible that these fluids exported isotopically light K from the melt, such that the remaining melt acquired a heavier K isotopic composition, as observed in sample NJ-22. Other processes, such as assimilation of fresh or altered wallrock, would complicate this picture, but may be essential to accounting for the fact that both light and heavy extreme K-isotope compositions are observed. The roles of these mechanisms remain speculative, but we highlight them as provisional explanations for the highly variable isotopic compositions that seem to be characteristic of only a subset of the lavas in our dataset.

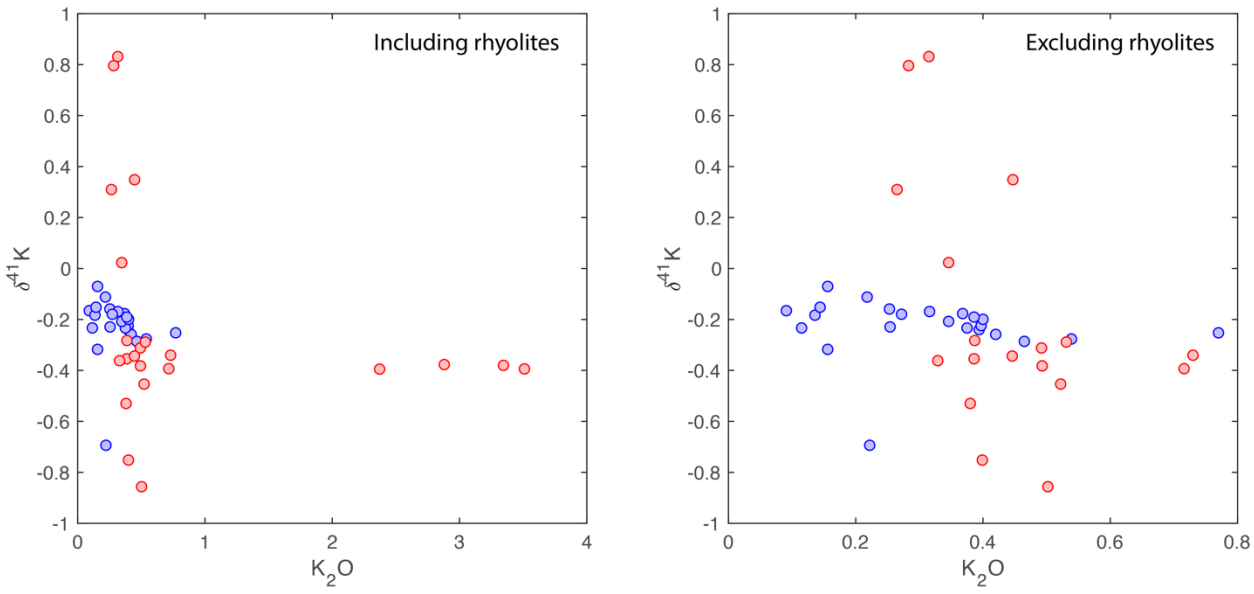

Overview of Izu arc-front (blue) and rear-arc (red) samples.

Section 2

Partition coefficients for Models 1 and 2

Partition coefficients used in Models 1 and 2 are included in Table S1 and S2, respectively.

Partitioning during MORB dehydration/melting

The partition coefficients for fluid loss from MORB are from the experiment at 4 GPa and 900 C of Kessel et al. (2005) for all elements except K. The starting material used by Kessel et al. (2005) was K-free. In the experiment, the elements Cs and Rb (the latter of which may commonly behave similar to K) are both highly incompatible — more so than even Pb and Sr. However, the mobility of Rb and K is expected to be sensitive to whether phengite is or is not saturated (Hermann and Rubatto, 2009), which in turn depends on several not well-constrained parameters—including temperature, the amount of fluid present, and the starting K content of the material. We therefore make a simplifying assumption: namely, that D(K) = D(Pb). Although we assign a saturation level of 40929 ppm K (~5 wt. % K_2O) in solution (see section on sediment melting), this has no effect for the MORB-derived fluid in our modeling—because the K content of the MORB-derived fluid does not quite reach that level in our modeling.

Partitioning during sediment dehydration/melting

The partition coefficients for fluid loss from sediment are from the experiment at C-1699 (3.5 GPa, 900 C) of Hermann and Rubatto (2009). In C-1699 and other experiments, K contents (as well as REE contents) of the melts are observed to not be well described by constant partition coefficients. Rather, the K abundance in the melt is buffered by phengite; the REE content by other accessory phases. The K content of the fluid is largely a function of T while phengite is present. In the experiments around 900 C (which is above the solidus), the K content of the melt is ~ 5 wt.% K_2O. We note that, as long as conditions are above the solidus, this value may not be expected to vary greatly—but even so K/Pb ratios may vary greatly with variable extents of melting because one element (K) would be buffered while the other (Pb) would have a variable abundance in the melt at different extents of melting. Thus, there may be large uncertainty in the estimated K/Pb ratios of the modeled sediment-derived fluids.

The partitioning of Pb was not estimated from the experimental data of Hermann and Rubatto (2009) because Pb alloying to gold capsules was observed during the experiments. In the experiments by Kessel et al. (2005) on MORB-type material, Pb is less compatible than Sr at lower temperatures (experiments at 4 GPa 700-800 C), whereas Pb and Sr are similarly incompatible near the transition from aqueous fluids to hydrous melts (experiments at 4 GPa 900-100 C). In Model 1, we assume D(Pb) = D(Sr) for sediment melting, which is consistent with these experiments. However, we use a different assumption in Model 2: D(Pb) = 2*D(Sr). The experiments on sediment melting of Johnson and Plank (1999) indicate greater compatibility of Pb than Sr in some cases, although there is a chance this is an artefact of Pb alloying. For example,

at 900 C, D(Sr) = 1.23 and D(Pb) = 1.29. We regard the partitioning of Pb during sediment melting to be somewhat uncertain, and therefore choose to use it as an adjustable in Model 2 in order to fit Pb- and Sr-isotope data.

Partitioning during fluid-mantle interaction

The partition coefficients for fluid-mantle interaction used only in Model 2 are based on the experiment at 6 GPa and 800 C of Kessel et al. (2005). The modelled trace-element patterns in the metasomatic fluid—and metasomatized mantle (Figure S1)—will be highly sensitive to the choice of partition coefficients. To explain the data, it is required that the fluid that interacts with the mantle incorporates high Pb contents while (1) not greatly fractionating Pb/Sr ratios relative to mantle-wedge composition and (2) fractionating Pb/LREEs and Pb/Nb ratios, such that Pb is much more highly concentrated than the LREEs and Nb in the fluid. The experimental data for the 6 GPa and 800 C experiment of Kessel et al. (2005) were used in the modeling because these partition coefficients result in Pb being highly mobilized while the LREEs and Nb are much less mobilized—and, hence, the elemental patterns are adequately fit (Figure S1).

Here we discuss possible alternative choices of partition coefficients. In the context of our model, partition coefficients for interaction between (hydrous) melts and mantle peridotite do not fractionate Pb/LREEs sufficiently. Higher rock-to-fluid ratios for the zone refining process would help this but would likely result in fractionation of other ratios (e.g., Pb/Sr) and thus not result in a better overall fit. Also, partition coefficients for relatively low pressures (900-100 C, 2 GPa; Ayers et al., 1997) appear to indicate greater compatibility of Sr in clinopyroxene, which would fractionate Pb/Sr ratios. As an alternative to the partition coefficients we used, the coefficients for the 4 GPa and 900 C experiment of Kessel et al. (2005) could be utilized (though for this experiment cpx compositions were not determined, so these coefficients would have to be scaled based on assumptions). These coefficients would be similar to those we used, except that (without rutile) they would indicate greater mobility for Nb, and hence not fit Nb well. Finally, the experiments of Adam et al. (2014) at 2 – 3 GPa and 1100-1200 C on fluids in equilibrium with peridotite indicate behavior capable of fractionating Pb (and Sr) from the LREEs but also indicate greater mobility for Nb. The viability of Model 2 may depend on whether under any conditions Pb (and other fluid-mobile elements) can be mobilized without also mobilizing LREEs and some HFSEs such as Nb.

Table S1

Model 1 — Partition coefficents and saturation levels

	MORB melting: D(solid/fluid)		MORB melting: Saturation level in fluid (ppm)		Sed. melting: D(solid/fluid)		Sed. melting: Saturation level in fluid (ppm)	
Pb	0.032	[1]	—		=1*D(Sr)	[2]	—	
Sr	0.047	[1]	—		0.10	[3]	—	
K	=D(Pb)	[2]	40929	[3]	—	[3]	40929	[3]
Nb	1.455	[1]	—		0.56	[3]	—	
La	0.8813	[1]	—		1.60	[3]	—	
Nd	0.6623	[1]	—		1.95	[3]	—	
Hf	1.926	[1]	—		0.91	[3]	—	
Yb	88.4	[1]	—		40.16	[3]	—	

[1] 4 Gpa, 900 C experiment of Kessel et al. (2005)

[2] Assumed

[3] experiment C-1699 (3.5 GPa, 900 C) of Hermann and Rubatto (2009)

Partition coefficients used in Model 2:

Table S2

Model 2 — Partition coefficents and saturation levels

	MORB melting: D(solid/fluid)		MORB melting: Saturation level in fluid (ppm)		Sed. melting: D(solid/fluid)		Sed. melting: Saturation level in fluid (ppm)		Mantle Fluid, Zone refining: D(solid/fluid)	
Pb	0.032	[1]	—		=2*D(Sr)	[2]	—	[1]	0.005	[4]
Sr	0.047	[1]	—		0.10	[3]	—	[1]	0.004	[4]
K	=D(Pb)	[2]	40929	[3]	—	[3]	40929	[2]	=D(Pb)	[2]
Nb	1.455	[1]	—		0.56	[3]	—	[1]	0.146	[4]
La	0.8813	[1]	—		1.60	[3]	—	[1]	0.010	[4]
Nd	0.6623	[1]	—		1.95	[3]	—	[1]	0.061	[4]
Hf	1.926	[1]	—		0.91	[3]	—	[1]	0.732	[4]
Yb	88.4	[1]	—		40.16	[3]	—	[1]	5.751	[4]

[1] Experiment (4 GPa, 900 C) of Kessel et al. (2005)

[2] Assumed

[3] Experiment C-1699 (3.5 GPa, 900 C) of Hermann and Rubatto (2009)

[4] Experiment (6 GPa, 800 C) of Kessel et al. (2005): grt/liq and cpx/liq partition coefficients and mantle-wedge peridotite composition with 5% garnet, 5% cpx

Section 3

Additional Details for Model 2 (control by slab and mantle components)

Elemental patterns:

A summary of model parameters and results for K, Pb, and Sr (elements and isotopes) is provided in **Table 2** of the main text. An expanded version of this table with concentrations of Nb, La, Nd, and Yb is proved in **Table S1** — This table also includes additional columns. The additional columns provide the elemental and isotopic compositions of the mixtures ("metasomatic fluids" in Table S1) of mantle-derived plus slab-derived fluids. The additional columns also provide the elemental and isotopic compositions of the metasomatized mantle—i.e., simple mixtures of the mantle-wedge and the metasomatic fluids. The mixing proportions used are 4% metasomatic fluid and 96% mantle wedge for the arc front, and 5% metasomatic fluid and 95% mantle wedge for the rear arc. Finally, plots showing elemental patterns for the metasomatized mantle are given in **Figure S1**.

Table S3

Expanded version of Table 2 from main text.

	Sed.	Sed. Fluid	MORB	MORB Fluid	A-F Slab Fluid	A-R Slab Fluid	A-F Mantle	A-F Mantle Fluid	A-R Mantle	A-R Mantle Fluid	A-F Metasomatic Fluid	A-R Metasomatic Fluid	A-F Metasomatized Mantle	A-R Metasomatized Mantle
Pb	15.4	69	0.51	9.9	39	69	0.016	2.0	0.027	3.5	3.8	6.6	0.2	0.4
Sr	136	1114	128	1938	1526	1114	4.9	656	7.3	973	698	980	33	56
K	9630.3	40929	1162	22630	31780	40929	16	1994	61	7666	3424	9262	152	521
206Pb/204Pb	18.63	18.63	18.31	18.31	18.59	18.63	17.91	17.91	17.94	17.94	18.25	18.29	18.22	18.26
208Pb/204Pb	38.63	38.63	37.74	37.74	38.52	38.63	37.70	37.70	37.79	37.79	38.11	38.21	38.07	38.18
87Sr/86Sr	0.7106	0.7106	0.7025	0.7025	0.7055	0.7106	0.7028	0.7028	0.7029	0.7029	0.7031	0.7034	0.7030	0.7033
d41K	-0.53	-0.07	-0.44	-0.13	-0.09	-0.07	-0.44	-0.44	-0.44	-0.44	-0.29	-0.36	-0.30	-0.37
Nb	5.220	9.130	3.620	2.504	5.817	9.130	0.035	0.236	0.184	1.257	0.504	1.635	0.053	0.257
La	23.400	14.763	4.190	4.742	9.752	14.763	0.078	6.796	0.220	19.171	6.938	18.959	0.352	1.157
Nd	25.200	13.021	10.660	15.933	14.477	13.021	0.447	7.385	0.604	9.981	7.725	10.126	0.738	1.080
Hf	1.440	1.573	2.460	1.290	1.431	1.573	0.135	0.184	0.149	0.204	0.244	0.270	0.139	0.155
Yb	2.530	0.064	3.280	0.038	0.051	0.064	0.306	0.053	0.246	0.043	0.053	0.044	0.296	0.236

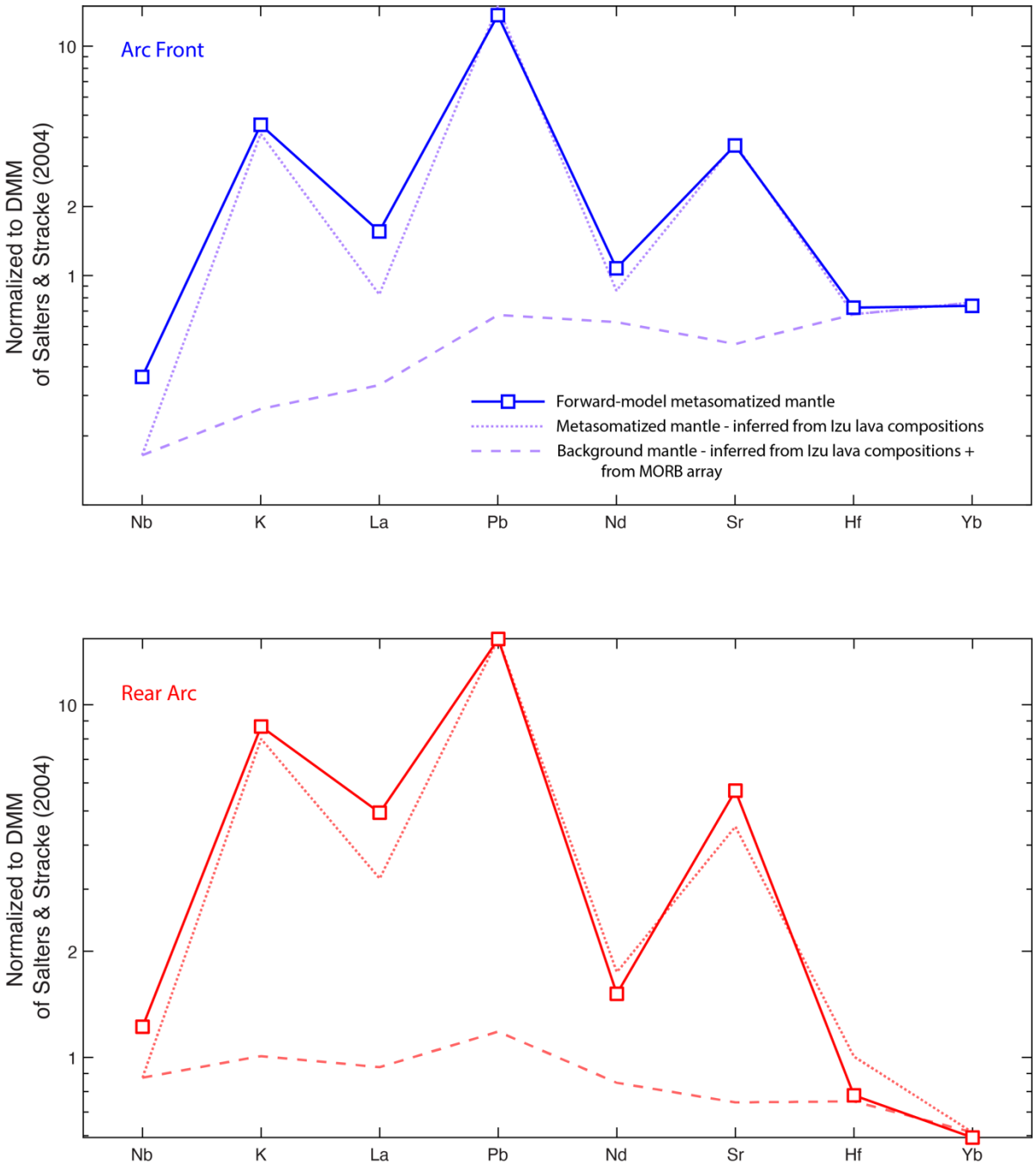

Figure S1. Modeled elemental pattern of Izu arc front and rear arc source mantle. The composition of metasomatized mantle obtained by forward modeling (Model 2) is shown by solid lines. The composition of metasomatized mantle as inferred from the Izu arc lava compositions is given by the dotted lines. The composition of the mantle wedge prior to addition of metasomatic fluid is given by the dashed lines. The method for inferring the metasomatized-mantle composition (as well as the mantle-wedge composition prior to metasomatism) is explained in the supplemental section "Composition of the mantle wedge".

Composition of mantle wedge

The elemental compositions of sub-arc-front and sub-rear-arc mantle wedge were estimated using an inverse calculation: namely, elemental data for primitive lavas (with 5.25 to 6.75 wt. % MgO) were used to estimate the composition of the mantle wedge. The following approach was taken. First, we took the elemental compositions of the primitive arc magmas (i.e., average composition using samples within the specified range of MgO) and scaled these concentrations by a factor of 0.7 to provide a rough correction for fractional crystallization of olivine: this calculation thereby provided us with estimates for the primary arc magmas for both the arc front and rear arc. Second, we assumed extents of melting, F, of the metasomatized mantle of 0.28 and 0.16 to produce the primary magmas of the arc front and rear arc, respectively. A higher extent of melting was assumed for the arc front than for the rear arc to be generally consistent with the significantly lower Nb contents and Nb/Yb ratios of the arc front relative to the rear arc. Here we used the mineral-melt partition coefficients from Salters and Stracke (2004), and a mantle (residue) mineralogy of 65% olivine, 30% orthopyroxene, 5% clinopyroxene, and 0% garnet. The mantle source composition was, thereby, calculated using the batch melting equation, and the specified F values and primary compositions. Third, X/Yb vs. Nb/Yb systematics (Figure 5) were used to estimate the enrichment factor for all elements for the arc front and rear arc: K, Pb, Sr, Nd, and Hf. We assumed enrichment factors of unity for both Nb and Yb, consistent with the assumption that these elements are negligibly affected by fluid contributions. These enrichment factors determine the proportion of each element that is endogenous to the mantle wedge vs. the amount that is added by metasomatic fluids. Thus, we used these factors, along with our estimates for the composition of the metasomatized mantle wedge, to produce estimates of the mantle wedge prior to metasomatism. In this way, we obtained the estimates for sub-arc-front and sub-rear-arc mantle wedge: These estimates were used in our modeling calculation and are listed in **Table S2**.

The radiogenic isotope composition of the mantle wedge was estimated on the basis on data for typical back-arc-basin basalts (BABBs) from the Shikoku Basin (Hickey-Vargas, 1991; Straub et al., 2010) as well as more enriched basalts from the Kinan Seamount Chain (Ishizuka et al., 2009). We assumed that the $^{143}Nd/^{144}Nd$ and $^{176}Hf/^{177}Hf$ ratios of the Izu arc lavas, in both the arc front and rear arc, may simply reflect the composition of the mantle wedge. Thus, we used the radiogenic-isotope compositions of typical BABBs to estimate the composition of the sub-arc-front mantle wedge, as these BABBs have $^{143}Nd/^{144}Nd$ ratios very similar to those of arc-front lavas. Also, we used radiogenic-isotope compositions (Pb, Sr, Nd, and Hf) midway between those of typical BABBs and basalts of the Kinan Seamount Chain to estimate the composition of the sub-rear-arc mantle wedge, as such $^{143}Nd/^{144}Nd$ ratios are similar to those of rear-arc lavas.

Zone-refining equations:

The 2nd model employs 'zone-refining' equations (e.g., Ayers, 1998). Note that, in the context of this model, the initial concentrations of the fluid are zero. As a result, the compositions obtained from a 'zone-refining' process at a high solid-to-liquid ratio (~200) are not much different from the compositions that would be obtained from a 'batch melting' process at a low degree of melting (~0.5%).

The zone-refining equations we used are as follows.

Equilibrium partition coefficients are defined as:

$$D = \frac{C_{solid}}{C_{fluid}}$$

The parameter, N, is the solid-to-fluid ratio. It describes the integrated amount of solid with which a parcel of fluid interacts.

The concentration of an element in the fluid is provided by:

$$C_{fluid} = C^{i}_{solid}/D_{s/f} - \exp(-ND_{s/f})\left(C^{i}_{solid}/D_{s/f} - C^{i}_{fluid}\right),$$

where the superscript "i" indicates "initial". C^{i}_{solid} and C^{i}_{fluid} are the initial concentrations in the solid and fluid, respectively. C_{fluid} is the final concentration in the fluid.

The radiogenic-isotope composition of a given element in the fluid is provided by:

$$\varepsilon_{fluid} = \frac{\left(C^{i}_{fluid}/C^{i}_{solid}\right)\varepsilon^{i}_{fluid} + \varepsilon^{i}_{solid}\left(1/D_{s/f}\right)\left[\exp\left(ND_{s/f}\right) - 1\right]}{\left(C^{i}_{fluid}/C^{i}_{solid}\right) + \left(1/D_{s/f}\right)\left[\exp\left(ND_{s/f}\right) - 1\right]}$$

where ε^{i}_{fluid} and ε^{i}_{solid} are the initial radiogenic-isotope ratios of the fluid and solid, respectively.

The stable-isotope composition of a given element in the fluid is provided by:

$$\delta_{fluid} = \frac{\left(C^{i}_{fluid}/C^{i}_{solid}\right)\delta^{i}_{fluid} + \left(\delta^{i}_{solid} - \Delta_{s-f}\right)\left(1/D_{s/f}\right)\left[\exp\left(ND_{s/f}\right) - 1\right]}{\left(C^{i}_{fluid}/C^{i}_{solid}\right) + \left(1/D_{s/f}\right)\left[\exp\left(ND_{s/f}\right) - 1\right]}$$

where δ^{i}_{fluid} and δ^{i}_{solid} are the initial stable-isotope compositions expressed as normalized ratios (delta values), and Δ_{s-f} is the difference fractionation factor ($\Delta_{s-f} = \delta_{solid} - \delta_{fluid}$).

Section 4 :

Statistics on δ^{41}K values

Difference in median δ^{41}K values: arc-front vs. rear-arc lavas

Medians, unlike means, are not highly sensitive to small numbers of outliers. Thus, we use medians to formalize the observation that, in general, the arc-front lavas have higher δ^{41}K values than do the rear-arc lavas. A 95% confidence interval was calculated for the difference between the medians. This interval was estimated by the percentile bootstrap method (Efron and Tibshirani, 1994). This was performed in the following way. First, we resampled from the δ^{41}K values of our arc-front dataset (n=24), drawing n times (randomly and with replacement). Second, we calculated a median from this "resample". We repeated steps one and two a large number of times (10^5), thereby generating 10^5 bootstrap estimates of the median for the arc-front lavas. These same steps were taken for the rear-arc dataset (n=22), generating 10^5 bootstrap estimates of the median for the rear-arc lavas. Finally, we calculated 10^5 differences by pairwise subtracting the bootstrap estimates of the rear-arc median from the bootstrap estimates of the arc-front median. **Figure S2** shows the resulting distribution. We obtain a 95% confidence interval for the difference between medians by taking the values at the 2.5th and 97.5th percentiles from this distribution.

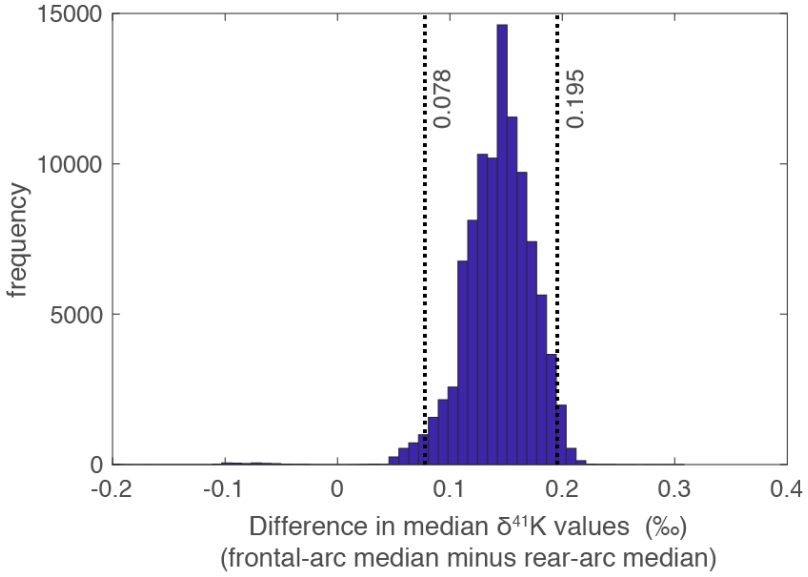

Figure S2. Bootstrap distribution of estimates of difference in median K-isotope composition between arc-front and rear-arc lavas.

Section 5:

Petrography on Sample NJ-22

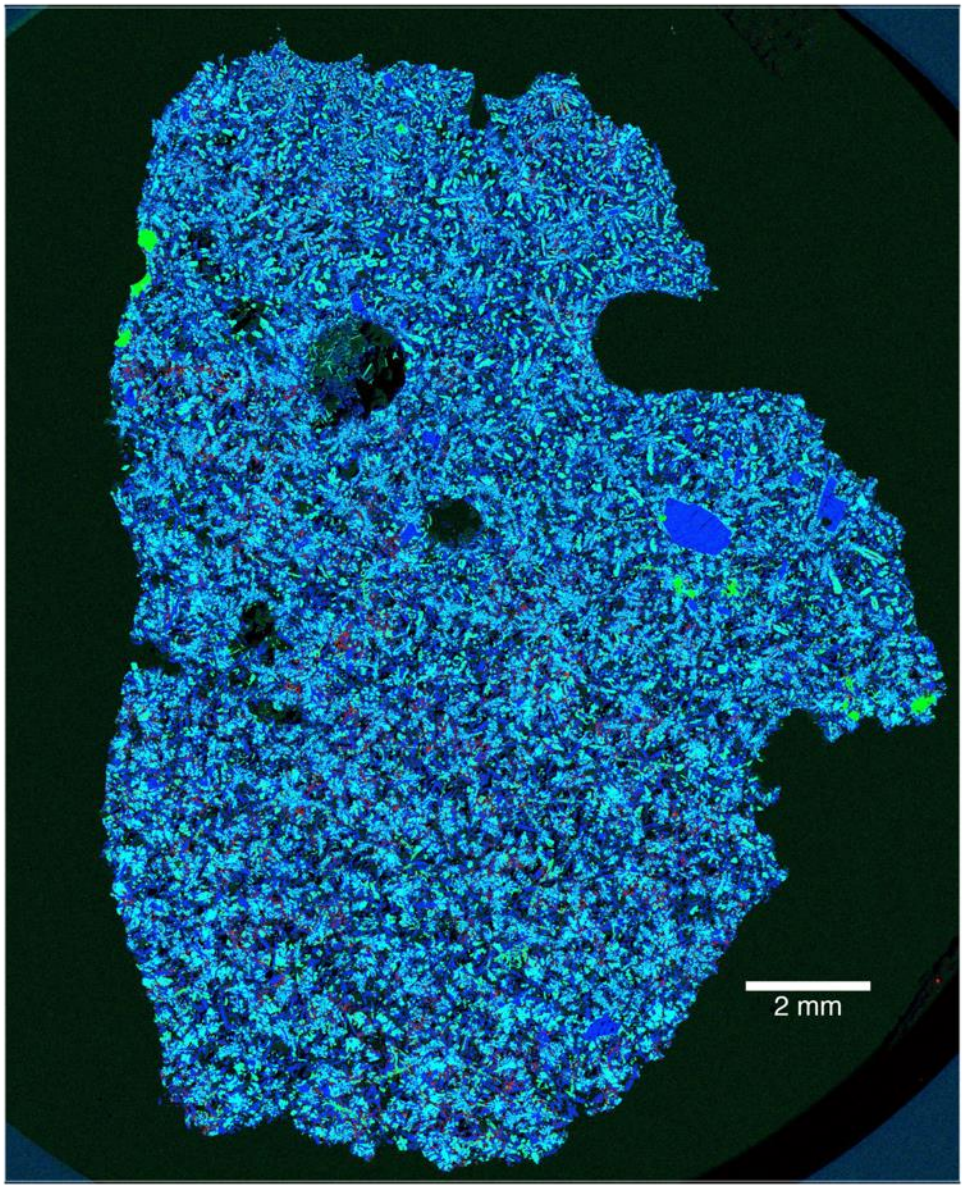

Figure S3. Combined elemental map of a polished section of sample NJ-22: K (red), Mg (green), and Ca (blue). Potassium is at highest concentrations in glass in interstices. Magnesium is mostly in pyroxene, and Ca is mostly in plagioclase.

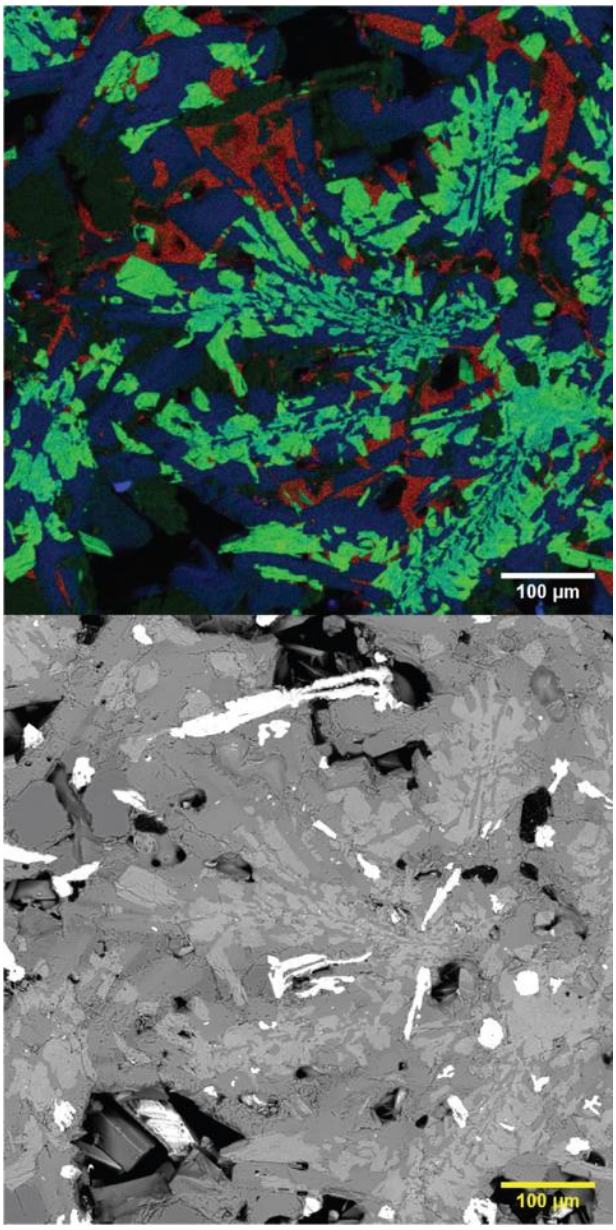

Figure S4. **(Top)** Combined elemental map of sample NJ-22 in a region of the section with interstitial glass: K (red), Mg (green), and Ca (blue). Potassium is apparent in glass. Magnesium is mostly in pyroxene, and Ca is mostly in plagioclase. **(Bottom)** Backscattered electron image of same region to show texture.

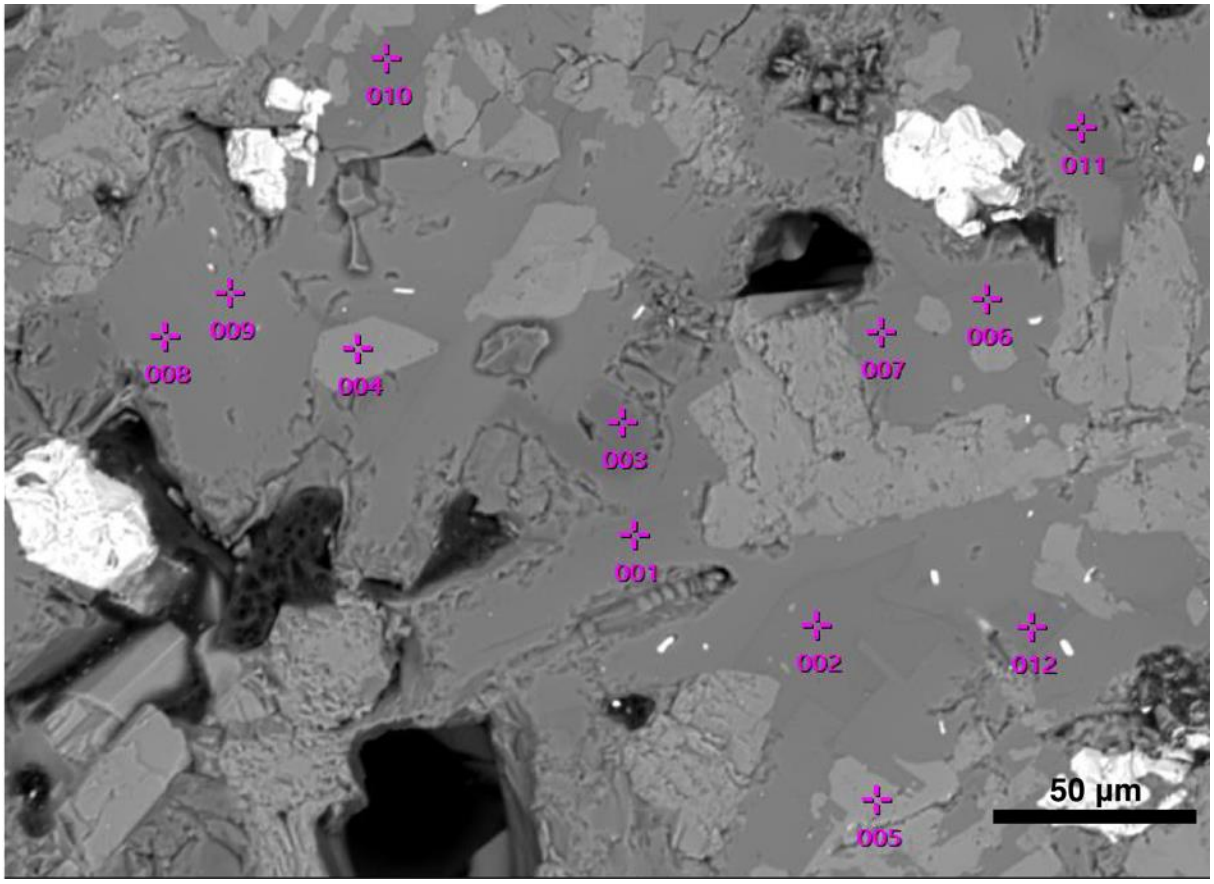

Figure S5. Backscattered electron image to show locations of point analyses on a part of sample NJ-22. Points 2, 10, and 12 have high K content. These points are interpreted as falling within areas of interstitial glass. Major elements compositions for these analyses are provided in **Table S4**.

#	Na2O	MgO	Al2O3	SiO2	K2O	CaO	TiO2	MnO	FeO
—	—	—	—	—	—	—	—	—	—
2	1.24		12.06	81.89	4.21	0.6			
—	—	—	—	—	—	—	—	—	—
4	2.19	14.26	11.8	43.51		10.86	2.61	0.54	14.22
5	0.7	11.2	7.85	44.9		21.77	1.52		12.07
6	4.3		28.37	53.85		13.48			
7	4.46		28.18	54.14		13.22			
8	4.13		28.46	53.73		13.68			
9	3.13		29.5	51.1		16.27			
10	1.2		12.25	82.34	3.52	0.69			
11	0.55			99.45					
12	1.31		11.84	82.41	3.87	0.57			

Table S4. Major element compositions (normed to 100 wt. % totals) obtained from analyses at locations indicated in previous figure. Points 2, 10, and 12 have high K content, and are highlighted. Other analyses (not shown) indicate that some plagioclase crystals (specifically,

1198 those with relatively sodic compositions) contain small amounts of K: up to roughly 0.06 wt. %
1199 K_2O.

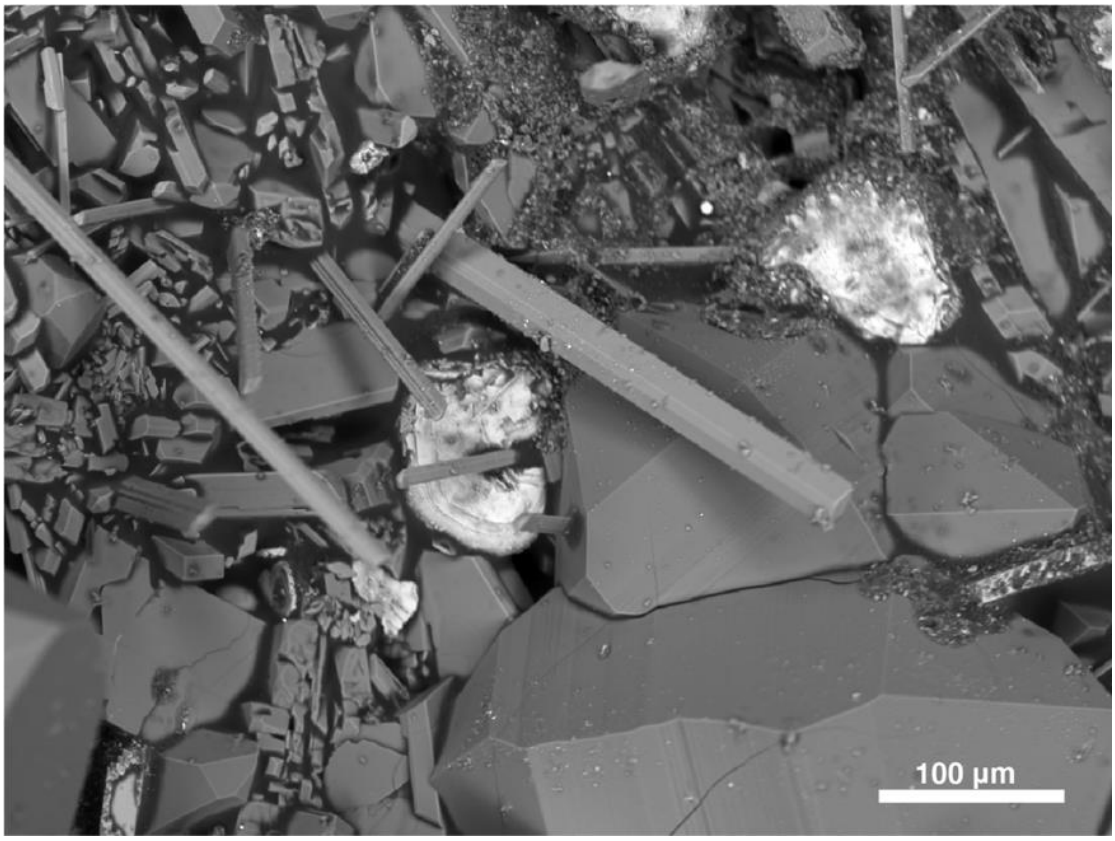

1200
1201 **Figure S6.** Backscattered electron image to show euhedral phenocrysts, mostly of plagioclase
1202 and pyroxene, in void space in sample NJ-22.

Section 6

K-Isotope Analytical Details

Conversion of $\delta^{41}K$ values between reference scales:

The following equation describes the conversion between δ-values relative to our lab standard ($\delta^{41}K_{Lab\_Standard}$) to δ-values relative to NIST SRM 3141a ($\delta^{41}K_{SRM\_3141a}$): $\delta^{41}K_{Lab\_Standard} = 1.000047 * \delta^{41}K_{SRM\_3141a} + 0.047$. It is sufficient to use $\delta^{41}K_{Lab\_Standard} = \delta^{41}K_{SRM\_3141a} + 0.047$. The conversion factor (0.047) was obtained by analyzing the standard NIST SRM 3141a relative to our lab standard (Figure S9).

Correction of $\delta^{41}K$ values for CaH^+ interference:

Testing revealed the presence of a Ca-hydride interference at mass 41, during analysis by MC-ICP-MS. This probably results from formation of a small amount of CaH^+ in the collision-reaction cell. Thus, we monitored the Ca content of solutions to ensure that Ca was sufficiently low in all solutions. This was done by collecting the mass-40 beam. We also applied small corrections to account for the effects of this interference on K-isotope ratios. The corrections were generally <15 ppm.

The corrections require knowledge of the ratio of $^{41}(CaH^+)$ to $^{40}Ca^+$ entering the Faraday cups. A solution of Ca-spiked stand14ard was measured relative to unspiked standard during almost every analytical session, so that this ratio could be independently estimated for each session. The ratio of $^{41}(CaH^+)$ to $^{40}Ca^+$ is given by: $^{41}CaH/^{40}Ca = (R_{spiked}^{41/39} - R_{std}^{41/39})/(R_{spiked}^{40/39} - R_{std}^{40/39})$, where R denotes the ratio of ion-beam intensities after blank subtractions: e.g., $R_{spiked}^{41/39} = (^{41}I_{spiked} - {}^{41}I_{blank})/(^{39}I_{spiked} - {}^{39}I_{blank})$. The error in $\delta^{41}K$ values of sample solutions arising from Ca-hydride interference is given by: $\delta^{41}K_{error} = 10^3 * R_{sample}^{40/41} * (^{41}CaH/^{40}Ca)$. The $\delta^{41}K$ values corrected for Ca-hydride interference are given by: $\delta^{41}K_{corrected} = \delta^{41}K_{uncorrected} - \delta^{41}K_{error}$.

Analytical uncertainty:

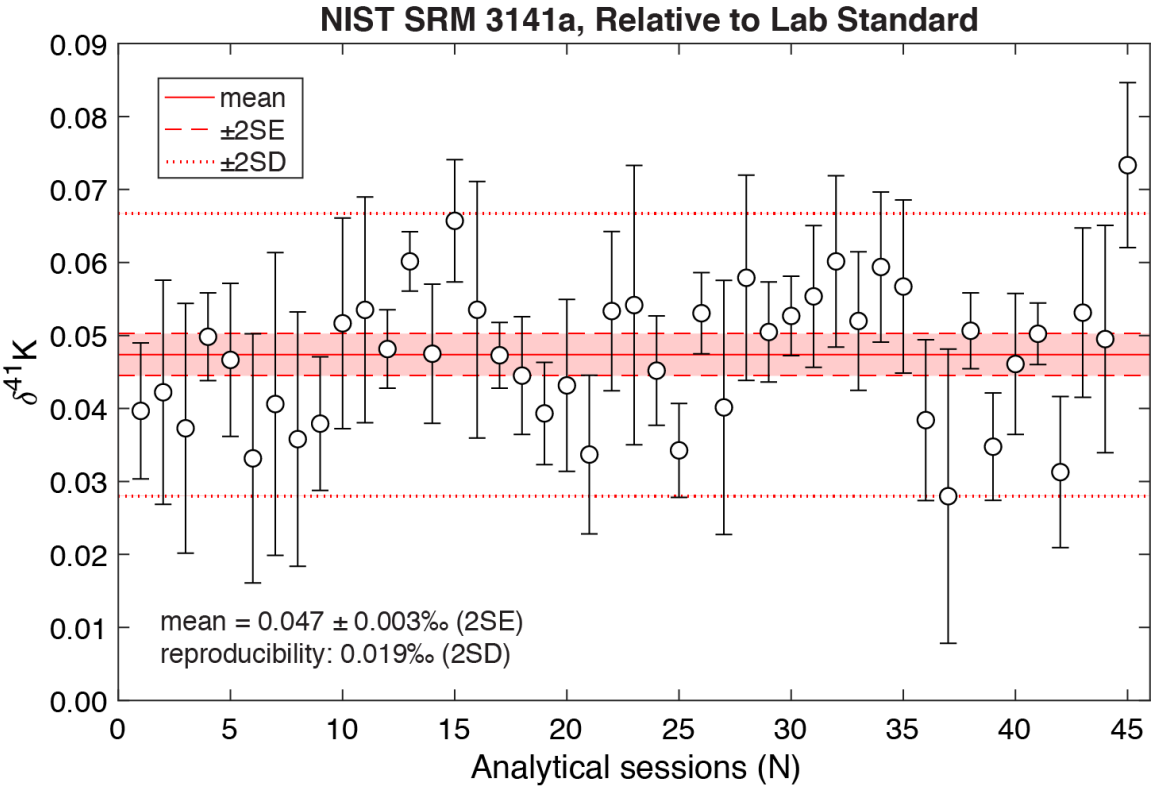

Figure S9. Measurements of NIST SRM 3141a relative to the lab standard of the Cosmochemistry Lab at Harvard University (Merck KGaA Suprapur high-purity KNO_3). Error bars on markers represent internal precisions (2SE). Data were collected over a 14-month period, from September 2018 to November 2019.

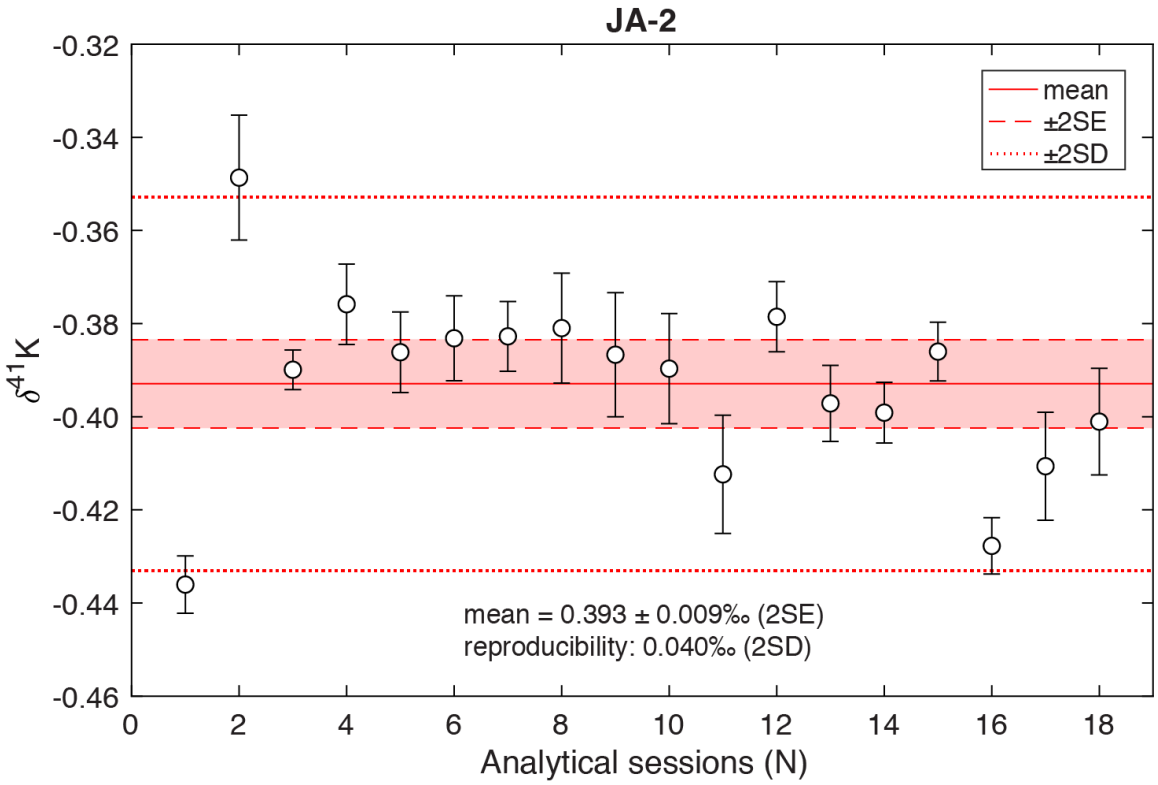

Figure S10. Measurements of Geological Survey of Japan standard JA-2, relative to the lab standard of the Cosmochemistry Lab at Harvard University. Markers represent instances in which separate aliquots of JA-2 were processed through columns and then measured during a single analytical session. Therefore, the data capture variability contributed by column chemistry. Error bars on markers represent internal precisions (2SE). Column separations were completed, and data were collected, over a 14-month period, from September 2018 to November 2019.

Ayers, J. C., Dittmer, S. K., & Layne, G. D. (1997). Partitioning of elements between peridotite and H2O at 2.0–3.0 GPa and 900–1100 C, and application to models of subduction zone processes. *Earth and Planetary Science Letters*, *150*(3-4), 381-398.

Ayers, J., 1998. Trace element modeling of aqueous fluid–peridotite interaction in the mantle wedge of subduction zones. Contributions to Mineralogy and Petrology 132, 390-404.

Chauvel, C., Marini, J.C., Plank, T., Ludden, J.N., 2009. Hf-Nd input flux in the Izu-Mariana subduction zone and recycling of subducted material in the mantle. Geochemistry, Geophysics, Geosystems 10.

Chavagnac, V., German, C., Taylor, R., 2008. Global environmental effects of large volcanic eruptions on ocean chemistry: Evidence from "hydrothermal" sediments (ODP Leg 185, Site 1149B). Journal of Geophysical Research: Solid Earth 113.

Durkin, K., Castillo, P.R., Straub, S.M., Abe, N., Tamura, Y., Yan, Q., 2020. An origin of the along-arc compositional variation in the Izu-Bonin arc system. Geoscience Frontiers 11, 1621-1634.

Efron, B., Tibshirani, R.J., 1994. An introduction to the bootstrap. CRC press.

Gale, A., Dalton, C.A., Langmuir, C.H., Su, Y., Schilling, J.G., 2013. The mean composition of ocean ridge basalts. Geochemistry, Geophysics, Geosystems 14, 489-518.

Green, T., Pearson, N., 1987. An experimental study of Nb and Ta partitioning between Ti-rich minerals and silicate liquids at high pressure and temperature. Geochimica et Cosmochimica Acta 51, 55-62.

Hauff, F., Hoernle, K., Schmidt, A., 2003. Sr-Nd-Pb composition of Mesozoic Pacific oceanic crust (Site 1149 and 801, ODP Leg 185): Implications for alteration of ocean crust and the input into the Izu-Bonin-Mariana subduction system. Geochemistry, Geophysics, Geosystems 4.

Hermann, J., Rubatto, D., 2009. Accessory phase control on the trace element signature of sediment melts in subduction zones. Chemical Geology 265, 512-526.

Hermann, J., Spandler, C., Hack, A., Korsakov, A.V., 2006. Aqueous fluids and hydrous melts in high-pressure and ultra-high pressure rocks: implications for element transfer in subduction zones. Lithos 92, 399-417.

Hermann, J., Spandler, C.J., 2008. Sediment Melts at Sub-arc Depths: an Experimental Study. Journal of Petrology 49, 717-740.

Hickey-Vargas, R., 1991. Isotope characteristics of submarine lavas from the Philippine Sea: implications for the origin of arc and basin magmas of the Philippine tectonic plate. Earth and Planetary Science Letters 107, 290-304.

Ishizuka, O., Yuasa, M., Taylor, R.N., Sakamoto, I., 2009. Two contrasting magmatic types coexist after the cessation of back-arc spreading. Chemical Geology 266, 274-296.

Johnson, M. C., & Plank, T. (2000). Dehydration and melting experiments constrain the fate of subducted sediments. *Geochemistry, Geophysics, Geosystems*, *1*(12).

Kelley, K.A., Plank, T., Ludden, J., Staudigel, H., 2003. Composition of altered oceanic crust at ODP Sites 801 and 1149. Geochemistry, Geophysics, Geosystems 4.

Kessel, R., Schmidt, M.W., Ulmer, P., Pettke, T., 2005. Trace element signature of subduction-zone fluids, melts and supercritical liquids at 120–180 km depth. Nature 437, 724-727.

Kimura, J.I., Kent, A.J., Rowe, M.C., Katakuse, M., Nakano, F., Hacker, B.R., van Keken, P.E., Kawabata, H., Stern, R.J., 2010. Origin of cross-chain geochemical variation in Quaternary lavas from the northern Izu arc: using a quantitative mass balance approach to identify mantle sources and mantle wedge processes. Geochemistry, Geophysics, Geosystems 11.

Parendo, C.A., Jacobsen, S.B., Wang, K., 2017. K isotopes as a tracer of seafloor hydrothermal alteration. Proceedings of the National Academy of Sciences, 201609228.

Plank, T., Kelley, K.A., Murray, R.W., Stern, L.Q., 2007. Chemical composition of sediments subducting at the Izu-Bonin trench. Geochemistry, Geophysics, Geosystems 8.

Salters, V.J., Stracke, A., 2004. Composition of the depleted mantle. Geochemistry, Geophysics, Geosystems 5.

Schmidt, M.W., Vielzeuf, D., Auzanneau, E., 2004. Melting and dissolution of subducting crust at high pressures: the key role of white mica. Earth and Planetary Science Letters 228, 65-84.

Scudder, R.P., Murray, R.W., Schindlbeck, J.C., Kutterolf, S., Hauff, F., McKinley, C.C., 2014. Regional-scale input of dispersed and discrete volcanic ash to the I zu-B onin and M ariana subduction zones. Geochemistry, Geophysics, Geosystems 15, 4369-4379.

Straub, S.M., Goldstein, S.L., Class, C., Schmidt, A., Gomez-Tuena, A., 2010. Slab and mantle controls on the Sr–Nd–Pb–Hf isotope evolution of the post 42 Ma Izu–Bonin volcanic arc. Journal of Petrology 51, 993-1026.

Taylor, R.N., Nesbitt, R.W., 1998. Isotopic characteristics of subduction fluids in an intra-oceanic setting, Izu–Bonin Arc, Japan. Earth and Planetary Science Letters 164, 79-98.

Tuller-Ross, B., Marty, B., Chen, H., Kelley, K.A., Lee, H., Wang, K., 2019. Potassium isotope systematics of oceanic basalts. Geochimica et Cosmochimica Acta 259, 144-154.

Declaration of interests

☒ The authors declare that they have no known competing financial interests or personal relationships that could have appeared to influence the work reported in this paper.

☐The authors declare the following financial interests/personal relationships which may be considered as potential competing interests:

CRediT author statement

C.P. and S.J. conceptualized and initiated the project. C.P. carried out analytical work, developed the interpretation with input from S.J., R.T., and J.K., and wrote the original draft of the manuscript. R.T. and J.K. provided materials. All authors discussed ideas and provided comments throughout the investigation and manuscript revision process.